

Width evolution of channel belts as a random walk

Jens M. Turowski^{1,2}, Fergus McNab¹, Aaron Bufe^{1,3}, Stefanie Tofelde⁴

¹ Helmholtz Zentrum Potsdam, GeoForschungsZentrum (GFZ) Potsdam, Potsdam, Germany

² State Key Laboratory of Hydrosience and Engineering, Tsinghua University, Beijing, China

³ Department of Earth and Environmental Sciences, Ludwig Maximilian University Munich, Munich, Germany

⁴ Institute of Geological Sciences, Freie Universität Berlin, Berlin, Germany

Correspondence to: Jens M. Turowski (jens.turowski@gfz-potsdam.de)

Abstract. Channel belts ~~—floodplains and fluvial valley floors—~~form by the mobilization and deposition of sediments during the lateral migration of rivers. Channel-belt width and its temporal evolution is important for the hydraulics, hydrology, and ecology of ~~floodplains~~[landscapes](#), and for human activities such as farming, protecting infrastructure, and natural hazard mitigation. Yet, we currently lack a comprehensive theoretical description of the width evolution of channel belts. Here, we explore the predictions of a physics-based model of channel-belt width for the transient evolution of channel belts. [The model applies to laterally unconfined channel belts in foreland areas as well as to laterally confined channel belts in mountain settings \(here, channel-belt width equals valley-floor width\)](#) The model builds on the assumption that the switching of direction of a laterally migrating channel can be described by a Poisson process, with a constant rate parameter related to channel hydraulics. As such, the lateral migration of the channel can be viewed as a non-standard one-dimensional random walk. [In other words, at each river cross section the river randomly moves either to the left or right at a given time.](#) The model predicts three phases in the growth of channel belts. First, before the channel switches direction for the first time, the channel belt grows linearly. Second, as long as the current width is smaller than the steady state width, growth follows an exponential curve on average. Finally, there is a drift phase, in which the channel-belt width grows with the square root of time. We exploit the properties of random walks to obtain equations for the distance from a channel that is unlikely to be inundated in a given time interval (law of the iterated logarithm), distributions of ~~first passage times~~[the channel requires to return to its origin and of the first arrival at a defined given position away from the origin—return to the origin](#), and the mean lateral drift speed of steady state channel belts. All of the equations can be directly framed in terms of the channel's hydraulic properties, in particular its lateral transport capacity that quantifies the amount of material that the river can move in lateral migration per unit time and channel length. ~~Finally~~[The ,we derive the](#) distribution of sediment ~~residence time~~[age within the channel belt is equivalent to the distribution of times to return to the origin, and show that it](#) which has a right-hand tail [that](#) follows a power-law scaling with an exponent of $-1.53/2$. As such, the mean and variance of ages of sediment deposits in the channel belt do not converge to stable values [over time](#), but depend on the time since the formation of the channel belt. This result has implications for storage times and chemical alteration of floodplain sediments, and the interpretation of measured sediment ages. ~~Our model~~ predictions compare well to data of sediment-age distributions ~~from various selected~~[measured at](#) field sites and the temporal evolution of channel belts observed in flume experiments. [Both comparisons indicate that a random walk approach adequately describes the lateral migration of channels and the formation of channel belts.](#) The theoretical description of the temporal evolution of channel-belt width developed herein ~~provides a framework in which observational data can be interpreted,~~[can be used for predictions for example in hazard mitigation and stream restoration, and to invert se](#)

40 fluvial strata for ambient hydraulics conditions. Further, it ~~and~~ may serve to connect models designed either for
41 long-geological and short process timescales.
42

43 1 Introduction

44 Rivers migrate laterally. Lateral river migration establishes the channel belt, which is defined as the corridor of
45 channel migration formed during one river-avulsion cycle (Bridge and Leeder, 1979; Nyberg et al., 2023).
46 Channel belts include the river channel and active bars, levees and abandoned channels, and other areas affected
47 by the river during floods or migration (Fig. 1a) (Nyberg et al., 2023). They can be represented by the planform
48 area that the river has interacted with since its last avulsion, and they can be Channel belts can be either
49 unconfined, for example in foreland areas, or confined, for example by valley walls in mountain regions (Fig. 1
50 a&b) (e.g., Howard, 1996; Limaye, 2020; Turowski et al., 2024). ~~During lateral migration, rivers deposit~~
51 ~~sediment or erode previously deposited sediment, thereby affecting chemical weathering, nutrient transport, and~~
52 ~~ecology (e.g., Fotherby, 2009; Jonell et al., 2018; May et al., 2013; Miller, 1995; Naiman et al., 2010; Schumm~~
53 ~~& Lichty, 1963; Torres et al., 2017).~~ Channel belts affect catchment hydrology, host aquifers and hydrocarbon
54 deposits (e.g., Andersen et al., 1999; Blum et al., 2013; Bridge, 2001), and present a key location for organic
55 carbon storage and alteration (e.g., Repasch et al., 2021). During lateral migration, rivers deposit sediment or
56 erode previously deposited sediment, thereby affecting chemical weathering, nutrient transport, and ecology (e.g.,
57 Fotherby, 2009; Jonell et al., 2018; May et al., 2013; Miller, 1995; Naiman et al., 2010; Schumm & Lichty, 1963;
58 Torres et al., 2017). ~~Landforms such as backswamps or oxbow lakes, which are specific to channel belts, often~~
59 ~~host unique ecological communities that depend on regular floods (e.g., Bayley, 1991; Junk et al., 1989; Meitzen~~
60 ~~et al., 2018).~~ Further, the exchange of sediment during lateral channel migration determines the distribution of
61 ages of the sediment stored at and near the surface along rivers, with implications for landscape dynamics, the
62 interpretation of fluvial stratigraphy, and nutrient cycles (e.g., Bradley & Tucker, 2013; Marr et al., 2000; Pizzuto
63 et al., 2017; Scheingross et al., 2021). Landforms such as backswamps or oxbow lakes, which are specific to
64 channel belts, often host unique ecological communities that depend on regular floods (e.g., Bayley, 1991; Junk
65 et al., 1989; Meitzen et al., 2018). Finally, lateral bank erosion is an important natural hazard that can destroy
66 agricultural areas and infrastructure (e.g., Badoux et al., 2014; Best, 2019). All of the mentioned effects make
67 channel belts an important component of river-fluvial response to environmental change (e.g., Hajek and Straub,
68 2017). As such, ~~they channel belts~~ record a river's past activity, and can be used as archives for Earth's history
69 on the timescale of hundreds to thousands of years (e.g., Allen, 1978; Bridge and Leeder, 1979). ~~Channel belts~~
70 ~~can be either unconfined, for example in foreland areas, or confined, for example by valley walls in mountain~~
71 ~~regions (Fig. 1 a&b) (e.g., Howard, 1996; Limaye, 2020; Turowski et al., 2024).~~

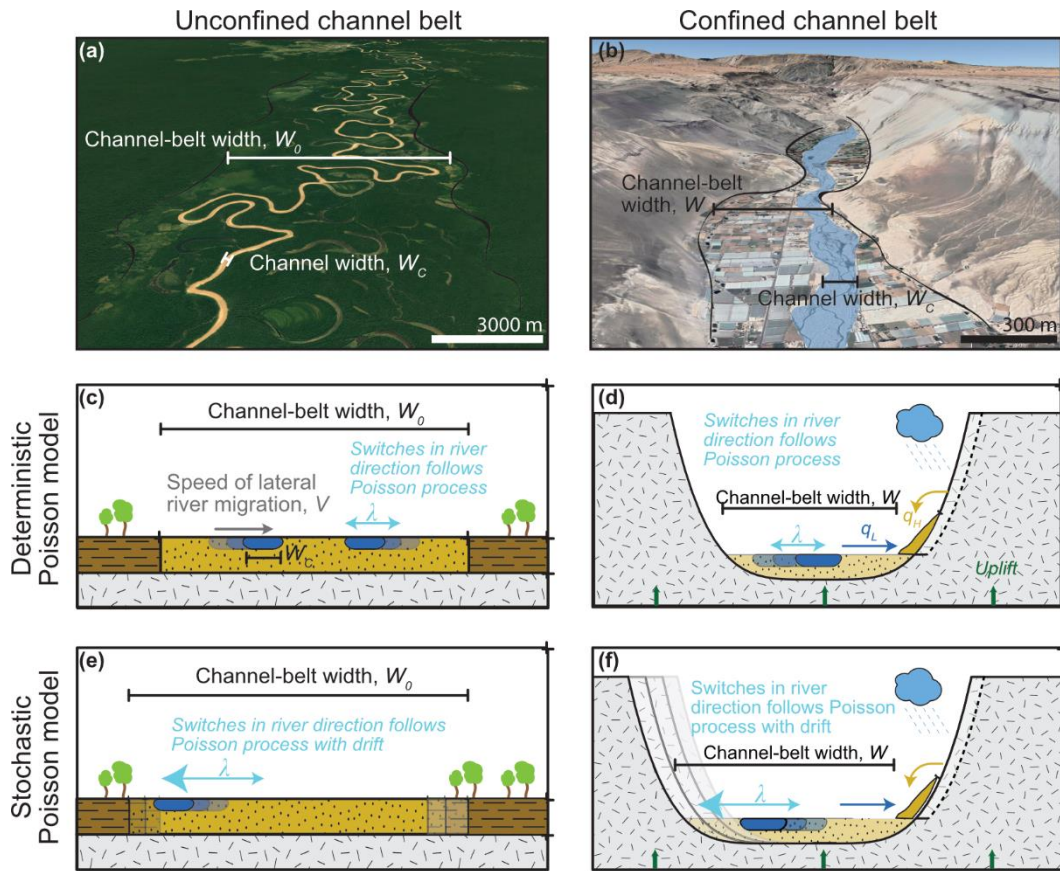
72
73 The long-term dynamics of channel belts have been studied separately for meandering (e.g., Camporeale et al.,
74 2005; Greenberg & Ganti, 2024; van de Lageweg et al., 2013) and braided rivers (e.g., Bertoldi et al., 2009;
75 Limaye, 2020). Researchers have largely focused on channel characteristics and statistics, their temporal evolution
76 and approach to a steady state. For meandering rivers, these have typically included the linear and curvilinear
77 wavelength, the curvature of the channel, and the role of meander cuts-offs in reaching and maintaining a steady
78 state (e.g., Camporeale et al., 2005; Howard, 1996). For braiding-braided rivers, they have typically included
79 braiding indices and planform patterns (e.g., Bertoldi et al., 2009; Egozi and Ashmore, 2009). In comparison to
80 these statistics describing the channels within the channel belt, the belt width has received little attention.
81 Greenberg et al. (2024) found that channel-belt area scales with floodplain reworking timescales. Reworking
82 timescales monotonically increase as water partitions into fewer active channel threads, and as channels become

83 more sinuous, and thus vary between river systems with different planform types. Studying models of meandering
84 rivers, Camporeale et al. (2005) concluded that one time and one length scale are sufficient to explain steady state
85 characteristics of channel belts regardless of the hydrodynamic complexity of the underlying model. They
86 suggested that channel-belt width scales with the meandering wavelength, which in turn scales with flow depth.
87 A qualitative comparison to natural channels was favourable. Limaye (2020) postulated that channel-belt width
88 of braided rivers scales with channel width. Using flume experiments, ~~they~~ he showed that both channel and belt
89 width follow a similar scaling relationship with discharge. Turowski et al. (2024) developed a steady state model
90 for confined and unconfined channel-belt ~~and valley~~ width under the assumption that switches in the direction of
91 lateral channel migration are based on a random process with a uniform mean rate of switching in time. In their
92 model, the unconfined steady state channel-belt width linearly depends on flow depth. The steady state width of
93 confined channel-belt (i.e., the valley-floor width) is reduced relative to unconfined channel belts due to lateral
94 input of sediments from adjacent valley walls. They also suggested that the steady state width of fluvial valleys is
95 controlled by the channel-belt width.

96
97 The ~~transient~~ temporal evolution of channel-belt width has so far hardly been explored. Limaye (2020) identified
98 three phases of channel-belt growth in his experiments, co-occurring with distinct phases of meandering or
99 braiding. In a first phase, the channel established a graded geometry from the initial imposed boundary condition.
100 In the second phase, the channel belt grew rapidly, while in the third phase, it reduced its growth rate. When
101 compared in a dimensionless framework, the switches between phases occurred at the same dimensionless time
102 for different experimental conditions. Wickert et al. (2013) and Bufe et al. (2019) observed an exponential
103 approach to the steady state width in experiments, when tracking the increase of the area visited by the channel
104 over time. Hancock & Anderson (2000) suggested that the initial rapid widening rate of a channel belt and the
105 subsequent decrease of the widening rate is due to the declining probability of the channel to be located at the belt
106 boundary as the belt widens. This notion was regularly picked up in subsequent work (e.g., Malatesta et al., 2017;
107 Martin et al., 2011), and has led to steady state descriptions of valley width (Tofelde et al., 2022; Turowski et al.,
108 2024). ~~Yet, e~~Equations relating the growth evolution of confined and unconfined channel belts ~~and valleys~~ to the
109 hydraulic conditions in the channel are currently not available. Yet, they could be useful in diverse topics. For
110 example, they could be used as forward models for making predictions related to flood hazard assessment and
111 stream restoration, or as inverse models to obtain paleo-hydraulic conditions from fluvial stratigraphy and
112 depositional sequences. Further, they could provide a framework to interpret data from natural rivers with regard
113 to nutrient cycling, channel-floodplain interactions, and ecology.

114
115 Turowski et al. (2024) described lateral channel migration as a Poisson process, in which the switches in direction
116 occur randomly in time at a constant mean rate. They subsequently focused on the mean behaviour of the model,
117 and proceeded to derive equations for the steady state width of unconfined and confined channel belts, ~~and of~~
118 fluvial valleys. Here, we explore the predictions of their model concept for the transient approach of channel belts
119 to their steady state width, and the consequences of a stochastic formulation for channel-belt dynamics.
120 Specifically, we derive analytical equations describing the temporal evolution and the bounds of channel belts,
121 their average lateral drift once they have reached a steady state, and the sediment residence-time distribution,
122 which is equivalent to the distribution of sediment ages. Analytical results are benchmarked with stochastic

123 numerical simulations. We compare the model results to data from flume two experiments (Bufe et al., 2016,
 124 2019), and sediment age distributions from three field sites (Everitt, 1968; Huffman et al., 2022; Skalak & Pizzuto,
 125 2010).



126
 127 **Fig. 1: Schematic illustration of the model concept.** a) Unconfined channel belt of the Juruá River, Brazil (6.75° S,
 128 70.30° W; Map data: Google, ©2024 Maxar Technologies). b) Confined channel belt of the San Jose River, Chile (18.58°
 129 S, 69.97° W; Map data: Google, ©2024 Maxar Technologies, Airbus). (c, d) the channel switches the direction of motion
 130 after a certain timescale. It thus evolves to a steady-state width that does not change over time. In the Stochastic
 131 Poisson Mmodel (e, f), the switching timescale is a random number. As such, the channel may migrate beyond the
 132 channel-belt limits (e) or erode the valley walls even after reaching the steady-state width. This migration can lead to a
 133 lateral drift of the unconfined or confined channel belt or the confined channel belt valley.

134 2 Theoretical developments

135 In this chapter, we will briefly summarize the valleywidth model by Turowski et al. (2024) (Section 2.1).
 136 Afterwards, we outline the basis of the stochastic model approach used herein (Section 2.2). Then, we derive
 137 equations for the temporal evolution of channel belts while approaching a steady state, and their lateral drift speed
 138 once they have reached steady state (Section 2.3), the limits of the channel-belt bounds (Section 2.4), the first
 139 passage distribution (Section 2.5), and the age distribution of sediment (Section 2.6).

140 2.1 Summary of the steady state model

141 Building on earlier work (e.g., Bufe et al., 2019; Martin et al., 2011; Tofelde et al., 2022), Turowski et al. (2024)
 142 developed a model for the steady state width of fluvial valleys (Fig. 1), which includes predictions for confined
 143 and unconfined channel belts as a special case. In the model, each cross-section contains a single channel, which

144 is treated as if it moves independently from those upstream and downstream. River channels are assumed to move
 145 laterally by bank erosion and deposition. The channel belt widens when the river crosses beyond the previous
 146 channel belt boundaries (Fig. 1). The lateral channel-migration speed V [$L T^{-1}$] is equal to the ratio of the lateral
 147 transport capacity q_L [$L^2 T^{-1}$] and the bank height in the direction of motion H_+ [L], where q_L quantifies the amount
 148 of material that the river can move in lateral direction per unit time and channel length (Bufe et al., 2019):

$$149 \quad V = \frac{q_L}{H_+}. \quad (1)$$

150
 151 Turowski et al. (2024) viewed switches in the direction of lateral motion of the river as stochastic events. These
 152 are assumed to be independent and identically distributed, with a constant mean event rate per unit time, λ [T^{-1}],
 153 and can therefore be described by a Poisson process. The mean rate of switching λ is equal-proportional to the
 154 ratio of the lateral transport capacity q_L and the square of the flow depth h [L] (Turowski et al., 2024)

$$155 \quad \lambda = k \frac{q_L}{h^2}, \quad (2)$$

156
 157 where k [-] is a dimensionless constant. We can define an effective switching time scale. This is as a constant time
 158 scale that leads to the same steady state width as is obtained from a fully stochastic model. The effective switching
 159 time scale ΔT [T] is inversely proportional to λ

$$160 \quad \Delta T = \frac{c}{\lambda}, \quad (3)$$

161
 162 where c [-] is a dimensionless constant of order one. Integrating over the distance travelled laterally by the channel
 163 within ΔT yields an equation for the unconfined channel-belt width W_0 [L] (see Turowski et al., 2024, for details):

$$164 \quad W_0 = \int_0^{\Delta T} V dt + W_C = k_0 h + W_C. \quad (4)$$

165
 166 Here, $k_0 = c/k$ [-] is a dimensionless constant, W_C [L] is the channel width, and t [T] is time. To arrive at the final
 167 equality in eq. (4), we assumed that in an unconfined channel belt that is neither incising nor aggrading, the bank
 168 height in the direction of motion, H_+ , is equal to the flow depth, h (cf. Turowski et al., 2024). In river valleys, the
 169 channel belt or valley floor is narrower than W_0 due to uplift or lateral supply of sediment from hillslopes, and the
 170 steady-state valley-floor width W_V [L] can be described by the equation (Turowski et al., 2024):

$$171 \quad W_V = \left(\frac{q_L - q_H}{U} \right) \ln \left\{ 1 + \frac{U(W_0 - W_C)}{q_L} \right\} + W_C. \quad (5)$$

172
 173 Here, q_H [$L^2 T^{-1}$] is the lateral supply rate of hillslope sediment per unit channel length, and U [$L T^{-1}$] is the uplift
 174 rate. Equation (5) predicts that river valleys reach a steady state width that depends on five input parameters (flow
 175 depth h , channel width W_C , uplift rate U , lateral transport capacity q_L , and lateral hillslope sediment supply q_H)
 176 and one constant (k_0) that needs to be determined from observations. Steady state valley width is reached when
 177 the system achieves a balance between local sediment input from hillslopes and by uplift, on the one hand, and
 178 the removal of sediment by the river, on the other hand.

179

180 In summary, in their model, Turowski et al. (2024) assume that the switches in river direction follow a Poisson
 181 process and unconfined channel belts evolve to a steady-state width determined by flow depth and channel width
 182 (eq. 4). Fluvial valleys can attain a maximum steady state width that corresponds to the unconfined channel-belt
 183 width W_0 . They are narrower than this unconfined width if they are affected by uplift or lateral hillslope sediment
 184 supply (eq. 5). We call this model the ‘Deterministic Poisson **Mmodel**’ hereafter.

185 2.2 The Stochastic Poisson **Mmodel**

186 In order to investigate the ~~transient-temporal~~ evolution of channel-belt width, we further develop the previous
 187 model of Turowski et al. (2024). Instead of ~~summarizing-assuming~~ the channel switches with a constant
 188 characteristic timescale, the effective switching timescale ΔT (eq. 3), we now explore the consequences of a
 189 random switching timescale. This consideration allows us to observe the ~~transient-temporal~~ behaviour of the
 190 random-walk model for lateral river migration. We call this model the ‘Stochastic Poisson ~~model~~’ **Model**
 191 hereafter. In a Poisson process, the probability mass function (PMF) that n [-] events (in this case, channel
 192 switches) occur within the ~~average switching timescale~~ ~~a time of length~~ Δt [T] is given by

$$193 \text{PMF}_{\text{Poisson}} = \frac{(\lambda \Delta t)^n e^{-\lambda \Delta t}}{n!}. \quad (6)$$

195 ~~Both (The expected number of events and their variance are~~ given by ~~$1/(\lambda \Delta t)$ [-] and the variance by $\lambda \Delta t$ [-]~~. For
 196 the derivations within this paper, we use the idea that the lateral motion of the river channel across the floodplain,
 197 in the model concept of a Poisson process, can be viewed as a non-standard one-dimensional random walk. The
 198 channel alternates between steps to the left and to the right within the cross section, thus switching direction after
 199 every step. The step length is not a constant, but a stochastic parameter equal to the waiting times between
 200 individual switching events multiplied by lateral migration speed. In a Poisson process, the waiting times T_w [T]
 201 between events are exponentially distributed with a mean waiting time of $1/\lambda$, a variance of $1/\lambda^2$, and a probability
 202 density function (PDF) given by

$$203 \text{PDF}_{\text{exponential } T_w} = \lambda e^{-\lambda T_w}. \quad (7)$$

205 Similarly, for constant migration speed V [L T⁻¹], the PDF of the length of steps $\Delta x = V \Delta t$ [L] is given by

$$206 \text{PDF}_{\Delta x \text{ exponential}} = \frac{\lambda}{V} e^{-\frac{\lambda}{V} \Delta x}. \quad (8)$$

208 In the following, we will first derive an equation for the approach to the steady state width using the ‘Deterministic
 209 Poisson **Mmodel**’ (Turowski et al., 2024), and then use the mathematics of random walks to explore the effects
 210 of stochasticity on the channel belt’s temporal evolution. Finally, we investigate the distribution of floodplain
 211 ages.

212 2.3 Temporal evolution of the channel-belt width

213 2.3.1 Approach to steady state in the ‘Deterministic Poisson **Mmodel**’

214 We first consider the evolution of the channel belt in an unconfined setting. Consider the river channel moving
 215 laterally with speed V . The channel belt widens when the river is located at and moves into the channel-belt

216 boundary. In contrast, if the river is not located at the boundary, or moves away from it, the channel-belt width
 217 remains unchanged. At any given time, widening can be observed with a probability P [-], which is equal to the
 218 fraction of the time the river spends widening the valley (e.g., Hancock and Anderson, 2002; Tofelde et al., 2022).
 219 The temporal evolution of channel-belt width W [L] is then governed by the differential equation (Tofelde et al.,
 220 2022)

$$221 \quad \frac{dW}{dt} = PV. \quad (9)$$

223 Motion in either direction is equally likely, and, for a given set of hydraulic, tectonic, and sedimentological
 224 boundary conditions, V can be considered as a constant (Bufe et al., 2019; Turowski et al., 2024). In a transient
 225 phase, before the steady state width is reached, the probability of the river not widening ~~(i.e., $1-P$)~~ the channel
 226 belt is equal to the ratio of the current W [L] and the maximum W_0 [L] channel-belt width (Tofelde et al., 2022).
 227 Channel width W_C provides a starting point and needs to be subtracted. Thus, P is given by (Turowski et al., 2024)

$$228 \quad P = 1 - \frac{W - W_C}{W_0 - W_C} = \frac{W_0 - W}{W_0 - W_C}. \quad (10)$$

230 The speed of lateral motion is equal to the ratio of the lateral transport capacity and the height of the bank in the
 231 direction of motion H_+ (eq. 1). Combining eqs. (1), (9) and (10), we obtain a differential equation for channel-belt
 232 evolution

$$233 \quad \frac{dW}{dt} = \frac{W_0 - W}{W_0 - W_C} \frac{q_L}{H_+}. \quad (11)$$

235 Solving equation (11) and applying the boundary condition that channel-belt width W is equal to W_C at time $t = 0$,
 236 we obtain

$$237 \quad W(t) = W_0 - (W_0 - W_C) \exp\left\{-\frac{t}{\tau}\right\} + W_C. \quad (12)$$

239 Here, τ is the governing timescale, which can be interpreted as a response time scale to an external perturbation
 240 (c-f. Tofelde et al., 2021). It is given by

$$241 \quad \tau = (W_0 - W_C) \frac{H_+}{q_L}. \quad (13)$$

243 ~~In the unconfined case, Assuming that~~ H_+ is equal to flow depth h and substituting eqs. (1) and (2) into eq. (11),
 244 we find that τ is equal to the effective switching time scale ΔT (see eqs. 3 and 4):

$$245 \quad \tau = \frac{c}{\lambda} = \Delta T. \quad (14)$$

247 We can use a similar approach to describe the evolution of a channel belt that is confined by valley walls when
 248 considering that at the valley walls, the lateral migration of the river slows down (cf. eq. 1). If the valley walls are
 249 made of alluvium, the bank height H_+ in eq. (9) is equal to the height of the valley wall H_W [L] and eq. (1) can be
 250 used as before. However, we need to adjust eq. (10), defining an equivalent probability $P_{confined}$ for a confined
 251 channel belt. The distance d [L] is the length that a channel moves on average across the valley floor in the

252 effective time ΔT [T] between two events of switching the direction of motion. This distance d is the sum of the
 253 distance covered at higher speed V when moving in the floodplain, and the distance covered when moving at
 254 lower speed v [L/T] when cutting into the valley walls (cf. Tofelde et al., 2022)

$$255 \quad d = V(1 - P_{confined})\Delta T + vP_{confined}\Delta T. \quad (15)$$

257 For the unconfined channel belt, we know that

$$258 \quad V\Delta T = W_0 - W_C. \quad (16)$$

260 Using eq. (16) to eliminate ΔT in eq. (15), and noting that d corresponds to the current width $W - W_C$, we obtain

$$261 \quad P_{confined} = \frac{W_0 - W}{(W_0 - W_C)\left(1 - \frac{v}{V}\right)} = \frac{W_0 - W}{(W_0 - W_C)\left(1 - \frac{H_W}{h}\right)}. \quad (17)$$

262 Here, we used eq. (1) to substitute for V and v , using $H_+ = h$ and $H_+ = H_W$, respectively. Note that in the assumption
 263 behind eqs. (15) to (17), $P_{confined}$ for a confined valley (eq. 17) reduces to P for an unconfined floodplain (eq. 8)
 264 for $v = 0$ or $H_W = 0$ (rather than $v = V$ or $H_W = h$). This arises from eq. (15), which yields $d = V\Delta T$ for $v = V$,
 265 rendering $P_{confined}$ meaningless. Substituting eq. (17) into eq. (9) and integrating again yields eq. (12) with a
 266 different governing timescale τ given by

$$268 \quad \tau = \frac{(W_0 - W_C)(H_W - h)}{q_L} = \left(\frac{H_W}{h} - 1\right)\frac{c}{\lambda}. \quad (18)$$

270 2.3.2 Channel belt evolution in the ⁴Stochastic Poisson model²

271 As we did in Section 2.3.1, we first consider the evolution of ~~the an unconfined~~ channel belt ~~in an unconfined~~
 272 ~~plane~~. In the ⁴Deterministic Poisson ~~M~~model², we obtained an exponential approach to the steady state width (eq.
 273 12) (Section 2.3.1). In the ⁴Stochastic Poisson ~~M~~model², we can distinguish three different phases in the growth
 274 of the channel-belt width over time. In the first phase, before the first switch in direction occurs, width increases
 275 linearly in time. In this phase, the growth rate is determined by the speed of lateral channel migration, V in the
 276 unconfined case and v in the confined case (see eq. 1 and Section 2.3.1). In the second phase, before reaching the
 277 steady state width, the channel-belt width grows exponentially on average. This average exponential growth can
 278 be described by the same equation (eq. 12) that has been derived for the ⁴Deterministic Poisson ~~M~~model² (see
 279 Section 2.3.1). In the third phase, which starts approximately when the width for the first time reaches the steady
 280 state width, stochastic drift dominates. Stochastic drift arises, because, due to the random motion of the channel,
 281 there is always a finite probability ~~to widen~~of widening the belt even after the steady state width has been reached.
 282 We already have equations for the linear (eq. 1) and the exponential (eq. 12) phase. In the following, we will fully
 283 exploit the stochastic properties of the model concept. In several of our considerations in this and the following
 284 sections, we use the central limit theorem, which states that the sum X of n stochastic variables with mean μ and
 285 variance σ^2 is normally distributed with mean $n\mu$ and variance $n\sigma^2$, if n is sufficiently large. In addition, we use
 286 the result that the sum or difference of two normally distributed parameters with means μ_1 and μ_2 and equal
 287 variance σ^2 follow a normal distribution with mean $\mu_1 \pm \mu_2$ and variance $2\sigma^2$.

288

289 First, we will derive an equation for widening during the drift phase using the evolution of random walks in the
 290 limit of a large number of steps. In this case, we can apply the central limit theorem. Thus, the PDF of the location
 291 of the channel can then be described by a normal distribution. In a random walk, the width of this normal
 292 distribution increases with the square root of its variance $\text{VAR}_{UCB} [L^2]$, where the subscript stands for ‘unconfined
 293 channel belt’ (e.g., Lawler & Limic, 2010):

$$294 \quad W_{Drift} = \sqrt{\text{VAR}_{UCB}} + W_C. \quad (19)$$

296 To find an equation for the variance, we will use the concept of a random walk making steps in alternating
 297 directions with exponentially distributed step length. We consider m pairs of a total of n steps, where each of the
 298 n steps covers an average distance of V/λ . The difference of two consecutive identically exponentially distributed
 299 steps in opposite directions is described by the Laplace distribution with zero mean and variance $2V^2/\lambda^2$, with the
 300 PDF

$$301 \quad \text{PDF}_L = \frac{\lambda}{2V} e^{-\frac{\lambda}{V}|x|}. \quad (20)$$

303 After each pair of two steps, the river is always in a position where it switches direction in the same way, for
 304 example from left to right. The switch in the other direction, from negative to positive, also follows eq. (20). In
 305 the limit of large m , the position of the river is given by the sum of the positions of many step pairs. The central
 306 limit theorem applies, and the normal approximation gives the distribution of locations where the river switches
 307 either from positive to negative or vice versa, with zero mean and a variance of $2m V^2/\lambda^2 = n V^2/\lambda^2$. Finally,
 308 the channel-belt width is the difference of the switching position on either side, so the final variance needs to be
 309 multiplied by a factor of two. Applying the law of large numbers, the distance covered in the sum of all steps is
 310 equal to the number of steps times the average step length V/λ . The average time of each step is the mean waiting
 311 time $1/\lambda$, and so we can write $n = \lambda t$:

$$312 \quad \text{VAR}_{UCB} = 2n \frac{V^2}{\lambda^2} = 2 \frac{t}{\lambda} V^2 = \frac{2}{k} q_L t. \quad (21)$$

314 Thus, we obtain ~~the drifted distance or~~ the width increase due to drift from eqs. (19) and (21) as

$$315 \quad W_{Drift}(t) = \sqrt{\frac{2}{k} q_L t} + W_C. \quad (22)$$

317 For a confined channel belt, during the time the river incises into the confining walls, the speed of widening drops
 318 to q_L/H_w , where H_w is the height of the confining wall, while it remains at q_L/h , as before, when the river moves
 319 laterally within the channel belt. The average speed of motion is given by the geometric average of the two speeds,
 320 \bar{V}

$$321 \quad \bar{V} = \sqrt{vV} = \sqrt{\frac{h}{H_w}} V. \quad (23)$$

323 We obtain the variance by replacing V by \bar{V} in equation (22), giving the variance VAR_{CCB} for a confined channel
 324 belt

325
$$\text{VAR}_{CCB} = 2t\bar{V}^2/\lambda = 2q_L th/kH_W$$

 326 (24)

327 As before, the width during the drift phase evolves as the square root of the variance, giving

328
$$W_{Drift}(t) = \sqrt{2\frac{t}{\lambda}\bar{V}^2} + W_C = \sqrt{\frac{2}{k}\frac{h}{H_W}q_L t} + W_C.$$

 329 (25)

330 2.3.3 Drift speed of channel belts and dimensionless scaling factor of the mean switching time scale

331 During the drift phase, the channel belt widens laterally, increasing the area that has been reworked by the channel
 332 with the square root of time (eq. 25). Yet, growth on one side of the channel belt makes it less likely that the
 333 channel moves close to the other side. As such, parts of the channel belt may be abandoned and, for example,
 334 reclaimed by vegetation (Fig. 1E). Similarly, in the case of a vertically incising river, the channel-belt width can
 335 stay at the steady state value W_V (eq. 5), while the entire belt is moving laterally, and uplift converts old parts of
 336 the channel belt to fluvial terraces. Here, we consider the case that the channel belt keeps its width constant at the
 337 steady state width, because any acquisition of area of the belt due to lateral motion on one side leads to the
 338 abandonment of an equivalent area on the other side. In this case, instead of widening, during the drift phase, the
 339 entire belt drifts laterally. We will now derive an equation for the average drift speed in this case. The average
 340 drifted distance in one direction, X_{Drift} , is equal to the square root of the variance, as before (cf. eq. 19). Because
 341 we consider a distance, rather than the width, it is smaller by a factor of two in comparison to eq. (25), giving

342
$$X_{Drift}(t) = \sqrt{\frac{1}{k}\frac{h}{H_W}q_L t}.$$

 343 (26)

344 The derivative of eq. (26) with respect to time, evaluated at the time when the valley reaches its steady state width,
 345 T_{SS} [T], gives the drift speed V_{Drift} [LT^{-1}]

346
$$V_{Drift} = \frac{1}{2}\sqrt{\frac{1}{k}\frac{h}{H_W}q_L T_{SS}}.$$

 347 (27)

348 At time T_{SS} , X_{Drift} is equal to the steady state width W_0 , and we can use eq. (26) to obtain

349
$$T_{SS} = k\frac{H_W}{h}\frac{(W_0 - W_C)^2}{2q_L}.$$

 350 (28)

351 Substituting eq. (28) into eq. (27) yields

352
$$V_{Drift} = \frac{1}{\sqrt{2}}\frac{h}{kH_W}\frac{q_L}{(W_0 - W_C)}.$$

 353 (29)

354 We can use eq. (29) to arrive at a further result, and calculate the constant of proportionality c between the
 355 switching time scale ΔT and the rate constant λ (eq. 3). The ratio of the drift speed V_{Drift} and the lateral migration
 356 speed of the channel V is the same as the fraction of time that the river spends widening the channel belt. This is
 357 equal to the area under a normal distribution outside one standard deviation from the mean, $V_{Drift}/V = 0.3173$.

358 Setting $h/H_W = 1$ and substituting $q_L = Vh$, we find

359
$$\frac{V_{Drift}}{V} = 0.3173 = \frac{1}{\sqrt{2}}\frac{h}{k(H_W - W_C)} = \frac{1}{\sqrt{2}c}.$$

360 (30)

361 Equation (30) therefore yields $c = 2.2285$.

362

363 2.4 Channel-belt limits

364 We can use the properties of random walks to make a statement about the distance beyond which the river will
365 rarely migrate over a given timescale. Knowledge of this distance may be useful to delineate zones for building,
366 or to assess in which areas the river is likely (or not) to interact with its surrounding, for example, by reworking
367 sediment or evacuating erosion and weathering products. In random walks, this distance is described by the law
368 of the iterated logarithm (e.g., Kolmogoroff, 1929), which is a limit theorem that sits ~~somehere~~ in between the
369 central limit theorem and the law of large numbers. In the limit of a large number of steps, this law provides an
370 envelope to the area that the river almost surely will not leave in its stochastic motion. Consider the sum S over
371 the distance travelled in n steps over dimensionless time t^* , which is a dimensionless stochastic variable with zero
372 mean. The law of the iterated logarithm gives an upper and lower bound for this sum with the equation

$$373 \quad S = \pm \sqrt{2t^* \ln\{\ln\{t^*\}\}}. \quad (31)$$

374 Here, \ln denotes the natural logarithm, and the plus and minus give the upper and lower bound, respectively. We
375 define the dimensionless step length $s = \lambda \Delta x / V$. This step length is a stochastic variable that is exponentially
376 distributed with a mean of zero and variance equal to one (compare to eq. 7). Because the random walk has to be
377 symmetric for eq. (31) to apply, we consider the sum S of $m = n/2$ pairs of steps, distributed according to the
378 Laplace distribution (eq. 4520). Normalizing with the square root of the variance of the Laplace distribution, the
379 dimensional distance is then given by $X = \sqrt{2}SV/\lambda$. This is the distance from the origin that the channel will
380 almost surely not cross within timescale t . The dimensionless time is given as $t^* = 2Vt/h$, where the factor of
381 two accounts for the pairs of steps. Putting everything together and adding half of the channel width, we obtain

$$382 \quad X(t) = \sqrt{2} \frac{SV}{\lambda} + \frac{W_C}{2} = \pm 2 \frac{h}{k} \sqrt{2 \frac{\lambda t}{k} \ln\left\{\ln\left\{2 \frac{\lambda t}{k}\right\}\right\}} + \frac{W_C}{2}. \quad (32)$$

385 2.5 First passage time distribution

386 We can derive another result that may be useful for planning and hazard mitigation purposes over long time scales;
387 ~~when considering regular, effective floods~~. The first passage time distribution (e.g., Redner, 2001) is the
388 distribution of times until the channel reaches a point that is located a distance b [L] from the channel's original
389 location for the first time. This ~~time~~ distribution can be used, for example, to calculate a lifetime distribution of
390 structures located a distance b from the river. In random walks, the first passage time distribution is given by a
391 Lévy distribution. The distribution PDF_{FP,R} of times T_{FP} [T] is given by:

$$392 \quad \text{PDF}_{FP,R}(T_{FP}) = \frac{|b|}{\sqrt{2\pi \frac{h}{H_W} \frac{q_L}{k} T_{FP}^3}} \exp\left\{\frac{-b^2}{2 \frac{h}{H_W} \frac{q_L}{k} T_{FP}}\right\}. \quad (33)$$

393

394 2.6 Sediment residence-time distribution

395 The probability distribution of residence times may be useful to calculate the age distribution of sediments. This
 396 is relevant, for example, for understanding weathering rates in river deposits or transfer times of sediment and
 397 carbon to the ocean (e.g., Repasch et al., 2021; Scheingross et al., 2019; Tofelde et al., 2021). The residence time
 398 distribution differs from the first passage distribution (Section 2.5), but can be derived from it. We start with a
 399 single step outward. The migrated distance Δx until the channel switches direction is then given by the exponential
 400 distribution (eq. 8). We can then use the first passage distribution (eq. 33) for the time to return to the origin by
 401 migrating again a distance $b = \Delta x$. Finally, we need to account for all possible Δx in the initial step. Assuming that
 402 the first step has to erode into the valley walls, the distribution PDF_{RT} for the time needed to return to the origin
 403 T_R [T] is then given by

$$404 \text{PDF}_{RT}(T_R) = \int_0^{\frac{h}{H_W} V t} \frac{\lambda}{\frac{h}{H_W} V} \exp\left\{\frac{-\lambda}{V} \Delta x\right\} \frac{|\Delta x|}{\sqrt{2\pi \frac{h}{H_W} \frac{q_L}{k} \left(T_R - \frac{\Delta x}{\frac{h}{H_W} V}\right)^3}} \exp\left\{\frac{-\Delta x^2}{2 \frac{h}{H_W} \frac{q_L}{k} \left(T_R - \frac{\Delta x}{\frac{h}{H_W} V}\right)}\right\} d\Delta x. \quad (34)$$

405
 406 Unfortunately, eq. (34) does not yield an analytical solution, but can be solved numerically. However, we can find
 407 an analytical limit for the right-hand tail, when T_R is large. Then, the integral reduces to

$$408 \text{PDF}_{RT}(T_R \gg 0) = \int_0^\infty \frac{\lambda}{\frac{h}{H_W} V} \frac{|\Delta x|}{\sqrt{2\pi \frac{h}{H_W} \frac{q_L}{k} (T_R)^3}} \exp\left\{\frac{-\lambda}{V} \Delta x\right\} d\Delta x = \frac{\lambda}{\sqrt{2\pi}} \left(\frac{h}{H_W} \lambda T_R\right)^{-3/2}. \quad (35)$$

409 We suggest an analytical approximation for the entire distribution (eq. 34) by assuming that, for small T_R , the
 410 PDF approaches a constant. Using this condition together with eq. (35) and fixing the integral to one, as required
 411 for any distribution, we obtain the function

$$413 \text{PDF}_{RT}(T_R) \approx \frac{1}{\sqrt{2\pi}} \frac{a \frac{h}{H_W} \lambda}{1 + a \left(\frac{h}{H_W} \lambda T_R\right)^{3/2}}, \quad (36a)$$

414 with

$$416 a = \left(\frac{3}{2}\right)^3 \left(\frac{3}{2\pi}\right)^{3/2}. \quad (36b)$$

418 3. Comparison of Testing the Stochastic Poisson Model predictions to numerical model, experiments and 419 field data

420 We test the model predictions in two separate ways. First, we use a stochastic random walk model to benchmark
 421 and check the analytical equations (Section 3.1), by explicitly using the random properties to calculate the
 422 distributions and the mean behaviour. Next to the analytical equations derived so far, this is an independent way
 423 of evaluating the Stochastic Poisson Model. We refer to this approach as the Stochastic Benchmark, and use it to
 424 check that the derivations of the analytical equations are correct. Second, we want to test the results with published
 425 experimental or field data. A full comparison of all of the results derived herein is beyond the scope of the paper.

426 Instead, we focus on scaling relationships that are indicative of random walks. Thus, we test whether channel belts
427 can be described as a random walk, and validate the fundamental modelling assumptions and the approach that
428 we used to derive the analytical equations. Two results are particularly suitable for this test. First, published
429 distributions of floodplain sediment ages (Everitt, 1968; Huffman, 2022; Skalak & Pizzuto, 2010) (Section 3.2)
430 allow us to measure the sediment residence time distribution and test the prediction of a $-3/2$ power-law scaling.
431 Second, the temporal evolution of channel belts in braided channel experiments (Bufe et al. 2016a,b, 2019)
432 (Section 3.3) allow us to extract the average channel-belt-width evolution during the drift phase and validate the
433 predicted square-root scaling of average width with time during this phase. Results are then compared to two
434 separate types of data: (i) published distributions of floodplain sediment ages (Section 3.2) (Everitt, 1968;
435 Huffman, 2022; Skalak & Pizzuto, 2010), and (ii) the temporal evolution of channel belts in the experiments of
436 Bufe et al. (2016a,b, 2019) (Section 3.3).y show that are expected from a random walk, which is se data can be
437 described by our model

438 **3.1 ~~Numerical model~~Stochastic Benchmark calculations**

439 To benchmark the analytical equations, we ~~We used~~ a stochastic numerical random walk model, the Stochastic
440 Benchmark, as an independent evaluation of the Stochastic Poisson Model to check the analytical equations. ~~The~~
441 Stochastic Benchmark builds on the same assumptions used to derive the analytical results, but explicitly generates
442 random step lengths of the channel in alternating directions, thereby generating random paths of channel
443 migrationspecifically a non-standard random walk with non-uniform, exponentially distributed step length in
444 alternating directions. ~~We ran the SSstochastic Poisson MBenchmark in many iterations, calculated the average~~
445 behaviour and the corresponding distributions of the properties, and compared them to the analytical results. ~~The~~
446 analytical equations and the results from the ~~sSPoisson MStochastic Benchmark~~ are both fully determined and
447 mutually independent, and there is no need to fit any free parameters. ~~All~~The ~~scripts~~ to run and evaluate the
448 Stochastic Benchmark and to generate the figures are available in the publication by M^cNab (2024). Except where
449 otherwise stated, we fixed channel width to zero, and all other free model parameters to one. For each ~~time~~ step,
450 the step length was randomly picked from an exponential distribution (eq. 7), and the lateral position of the channel
451 was tracked by alternately adding or subtracting the obtained step length from the channel's previous position.
452 Channel-belt width was calculated as the difference of the maximum distance that the channel had migrated ~~into~~
453 in the positive and negative directions from the origin up to the time step of interest. In this way, we generated a
454 total of 1,000 trajectories of position and channel-belt width, each with a total length of 3,000 time steps. We
455 repeated this exercise for ratios of valley depth to channel depth of $H_w/h = 1, 10$ and 100 , for unconfined,
456 moderately and highly confined scenarios, respectively. We obtained the average position of the channel for bins
457 spaced logarithmically in time. We used the unconfined width in further simulations to check the drift equation
458 (eq. 25). For this check, we ran the ~~random walk~~Stochastic Benchmark, limiting the channel-belt width to the
459 steady-state width by adjusting the ~~other one~~ side of the valley in an equal manner when the channel ventured
460 beyond the channel-belt limit on ~~one the other~~ side ~~of it was eroded~~. This procedure results in a valley of fixed
461 width that moves laterally. We measured drift velocity for different steady state widths by varying the channel
462 depth, for different values of the lateral transport capacity, and, as above, for ratios of valley depth to channel
463 depth of $H_w/h = 1, 10$ and 100 , as before. These simulations were run for a total of 3,000 time steps to ensure
464 statistical convergence. To verify the dimensionless scaling factor c that relates the mean switching time to the

465 rate constant λ by c/λ , we compared the unconfined steady state width for various conditions to flow depth (eq. 2)
466 for simulations with $k = 1$. To obtain an independent estimate of W_0 from the data, we fitted the exponential
467 evolution equation (eq. 12) to the initial phase of channel-belt widening. To obtain the first passage distribution,
468 we ran 10,000 simulations, each until the walk reached a dimensionless distance of 10 from the starting point.;
469 and We used the results to construct the first passage distribution. ~~the distribution of channel belt ages, we ran the~~
470 ~~same random walk simulations until the channel returned to the origin for the first time. We repeated the~~
471 ~~simulation 10,000 times, for a maximum of 100,000 steps. The times needed to return to the origin in each run~~
472 ~~was used to construct the distribution of sediment residence times.~~ Similarly, to test the distribution of channel
473 belt ages, we ran the same random walk simulations until the channel returned to the origin for the first time. We
474 repeated the simulation 10,000 times, for a maximum of 100,000 steps. The times needed to return to the origin
475 in each run was used to construct the distribution of sediment residence times. ~~the first passage distribution, we~~
476 ~~ran 10,000 simulations, each until the walk reached a distance of 10 from the starting point. All scripts are~~
477 ~~available in the publication by McNab (2024).~~

478 3.2 Floodplain ages from the field

479 The -3/2 scaling in the distribution for the time needed to return to the origin (eqs. 34-36) is indicative of random
480 walks, and thus its presence in natural data is/would be a strong indication that this modelling approach is suitable
481 for describing the dynamics of channel belts. Yet, the controls on sediment ages in natural rivers can be
482 complicated. Depending on the location, sediments may not only be only deposited by laterally migrating
483 channels, but also by overbank deposition, tributaries, or other processes such as soil erosion or debris flows. We
484 thus do not expect the sediment age distribution in every river to follow the prediction of our model (eqs. 34-36).
485 To compare to predictions, we picked three channels with published age distribution that feature conditions close
486 to the assumptions of the model: single thread channels undisturbed by processes other than fluvial deposition
487 and erosion (e.g., debris flows), without major tributaries in the study area. We digitised floodplain ages published
488 by Everitt (1968) for the Little Missouri River at Watford, North Dakota, USA, by Skalak & Pizzuto (2010) for
489 the South River near Waynesboro, Virginia, USA, and by Huffman et al. (2022) for the Powder River between
490 Moorhead and Broadus, Montana, USA, to compare against the predicted power-law scaling (eq. 35). In the
491 original study of Skalak & Pizzuto (2010), the cumulative distribution function (CDF) of floodplain ages is shown
492 (their Figure 8). We estimated the PDF by numerically differentiating the CDF using a centred finite-difference
493 scheme. Note that Skalak & Pizzuto (2010) already reported a power law scaling with an exponent close to -3/2
494 in their study, while both Everitt (1968) and Huffman et al. (2022) interpreted their data using an exponential
495 function.

496 3.3 Analog Experiments

497 We further validate the model using against experimental data of Bufe et al. (2016a) and Bufe et al. (2019).
498 Primarily, we seek evidence for the drift phase, i.e., the increase of the average channel-belt width with the square
499 root of time with time in the later parts of the experiments. This would be a strong indication that channel belt
500 development can be described as a random walk. Bufe et al. (2016a) and Bufe et al. (2019) conducted and analysed
501 experiments on braided alluvial channels in a basin with dimensions of 4.8×3.0×0.6 m and filled with well-sorted
502 silica sand ($D_{50} = 0.52$ mm). Water and sediment were supplied into the basin at a constant rate from the centre

503 of one of the short edges, and flowed out of the opposite side of the basin across a weir into a drain. After the start
504 of the experiments, the system evolved into an aggrading braided channel network. Once the average aggradation
505 rate dropped to below 20% of the input flux, a flexing metal sheet underneath the basin was used to simulate an
506 uplifting fold. Here, we focus on 25 hours of data that was collected before the onset of uplift from Run 5, and on
507 55 hours of data from Run 7, an experiment without uplift (see Bufe et al., 2019, for more detail). Water discharge
508 was set to 790 ml/s in both experiments and sediment supply was 15.8 ml/s in Run 7 and 2.4 ml/s in Run 5.
509 Positions of the channels were tracked at one-minute intervals in overhead images by using blue-dyed water (Bufe
510 et al., 2016a) and were used to measure the rate at which the area reworked by the channel expanded over time
511 (Bufe et al., 2016a).

512 4. Results

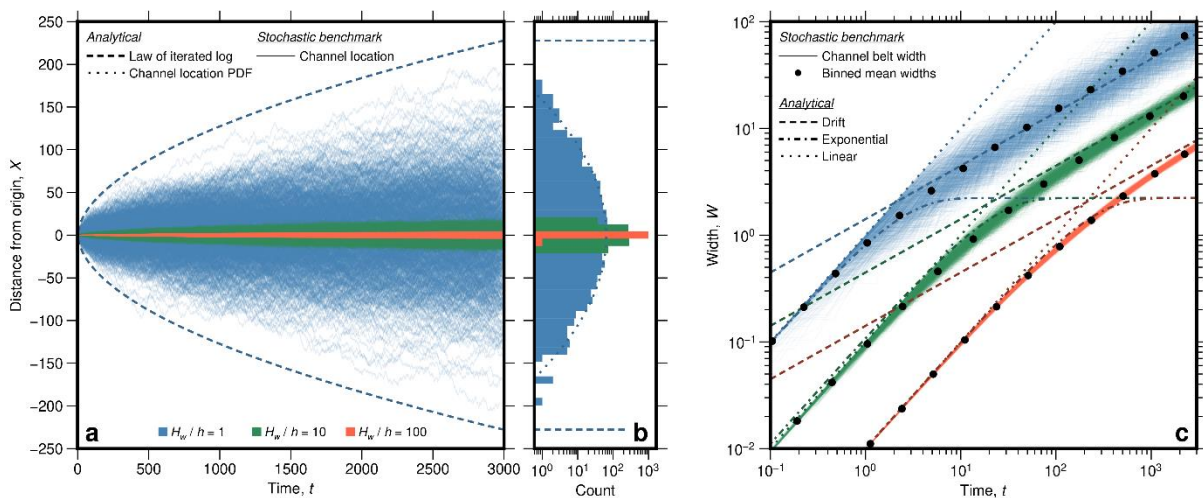
513 In general, our analytical solutions (section 2) agree well with the ~~Monte Carlo simulations of the random~~
514 ~~walks~~ Stochastic Benchmark (section Section 3.1) (Figs. 2-6), mostly yielding $R^2 > 0.99$ (Table 1). First, we
515 compare ~~can compare the channel location of the channel in the Stochastic Benchmark numerical random walk~~
516 ~~model with the~~ The law of the iterated logarithm (eq. 32) that gives an upper bound on the locations of the channel
517 through time (Fig. 2a,b), and the expected gaussian distribution of locations (Fig. 2b). After 3,000 steps, no
518 simulated random walk lies outside the predicted bounds (Fig. 2a,b, Fig. 5a, Fig. 6a), and the gaussian provides a
519 good description of the locations ($R^2 = 0.9962$). Further, ~~and we~~ we can derive the total width of the channel
520 belt in the simulations as the difference between the two outermost points visited by each random walk (Fig. 2c).
521 The temporal evolution of these widths identify all shows all three phases – linear increase, exponential increase
522 and square root drift – in the average temporal evolution of width, and that are expected by the random walk model,
523 and the analytical solutions predict the average behaviour well (Fig. 2c), with R^2 values exceeding 0.99 (Table 1).
524 ~~Passed the exponential growth, the widening rate of the channel belt slows. Here, we defining~~ Keeping the channel-
525 belt width constant at the steady-state channel-belt width as the width reached beyond the exponential growth
526 phase (see Fig. 2e). Then, we can measure a displacement of the channel belt with respect to the origin in the
527 Stochastic Benchmark numerical experiments (Fig. 3a), and calculate an average lateral ~~The lateral~~ drift velocity
528 for each experiment. We find that the average drift velocity of valleys at steady state is inversely proportional to
529 valley the steady-state channel-belt width and proportional to the lateral transport capacity (Fig. 3b&c). The
530 relationships agree with the prediction of ~~This proportionality is also predicted by the analytical solution~~, as
531 expected from eq. (29) (dotted lines in Fig. 3b&c) with R^2 values of 0.9999 (Table 1) (dotted lines in Fig. 3b,c).
532 Further, we find that ~~The theoretical value of the constant $c = 2.2285$ (eq. 30) could be verified by the~~
533 ~~simulations~~ The steady state widths of the simulated unconfined random walks increases as a function of the
534 increase linearly with channel depth following a power-law with an exponent of $c = 2.2285$ as predicted by eq.
535 30 (Fig. 4), with $R^2 = 0.9997$ (Table 1).
536 ~~with a gradient corresponding to $c = 2.2285$, as predicted (eq. 30) (Fig. 4).~~ The first passage distribution (eq.
537 33) describes the time for the random walk to reach a given distance from the origin and is plotted in Fig. 5a for
538 the Stochastic Benchmark numerical results. Again, the numerical results channel does not cross the theoretical
539 bound given by the law of the iterated logarithm (dashed line in Fig. 5a). Moreover, ~~The mean first passage time~~
540 ~~in the Stochastic Benchmark numerical results~~ is well fit by the analytical prediction of eq. (33) provides a good
541 description for the simulation results (Fig. 5b), with $R^2 = 0.9991$ (Table 1).

542 We found a similar correspondence between the Stochastic Benchmark numerical results, the bounds from the
 543 law of the iterated logarithm, and the theoretical-analytical solutions exists for the The distribution of times to
 544 return to the origin (Fig. 6a-&b), with $R^2 = 0.9953$ (Table 1). The analytical exact and approximate solutions of
 545 the Stochastic Poisson Model (eq. 34-35) (eq. 34) predicts a monotonically declining probability density with
 546 increasing return times (Fig. 6b). The analytical approximation of the age distribution (eq. 36, Fig. 6b)
 547 underpredicts the modelled-ages modelled by the Stochastic Benchmark for small ages in comparison to the exact
 548 solution, but provides an exact description of the right-hand power-law tail (Fig. 6b).

549
 550 Our The scaling predicted in the analytical equations model predictions also agree well with the selected a field
 551 and experimental datasets. First, the $-3/2$ power-law scaling (eq. 35) for the distribution of times to return to the
 552 origin are consistent with the data The age data from the Little Missouri River at Watford, North Dakota, USA
 553 (Everitt, (1968), the South River near Waynesboro, Virginia, USA (Skalak & Pizzuto, (2010), and the Powder
 554 River between Moorhead and Broadus, Montana, USA (Huffman et al., (2022) are consistent with the $-3/2$ power-
 555 law scaling (eq. 35) (Fig. 6e7; $R^2 = 0.8434$, 0.5576 and 0.8168 and 0.5576 , respectively). Second,

556
 557 In the evolution of the experimental channel belts in analog experiments, we can clearly identify a drift phase
 558 (Fig. 68). This phase is apparent as a square root scaling of channel-belt width as a function of time (eq. 25). We
 559 find $q_l/k = 2.15 \times 10^{-5} \text{ m}^2/\text{s}$ for Run 5 ($R^2 = \text{XXX}0.9995$) and $q_l/k = 2.62 \times 10^{-5} \text{ m}^2/\text{s}$ for Run 7 ($R^2 = \text{XXX}0.9960$).
 560 The investigated measured age distributions are consistent with the predicted $-3/2$ power law scaling. This will be
 561 discussed in detail in section 5.3. The evolution of average channel belt width in experiments shows the square
 562 root scaling with time, as expected for the drift phase (Fig. 7). The exponential phase approach (eq. 12) can also
 563 be fitted independently (see Bufe et al., 2019). However, the data resolution is not good enough to fit both
 564 relationships with consistent parameter values. Essentially, the resulting unconfined channel-belt width W_0
 565 depends on the subjective choice of which data points to include into the fit.

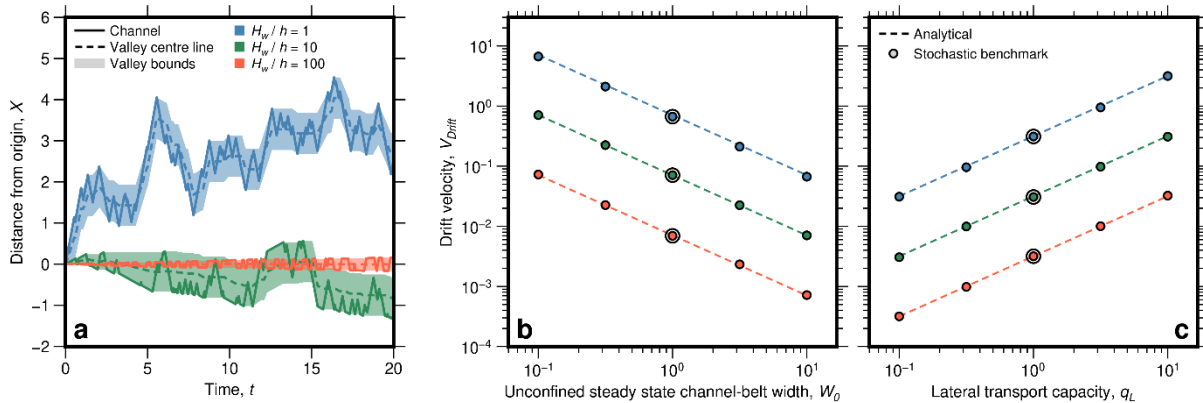
566
 567



568
 569 **Fig. 2: Temporal evolution of channel-belt width in the Stochastic Benchmark numerical experiments and comparison**
 570 **between the Stochastic Benchmark numerical experiments and the analytical solutions.** a) Modelled migration paths
 571 **through time (coloured solid lines), bounded by the law of the iterated logarithm (dashed line, eq. 32), i.e., the area that**
 572 **the river almost never surely does not crosses. Similar plots with longer runtimes can be found in Fig. 5a and Fig. 6a.**
 573 **The blue lines show the evolution of an unconfined river ($H_w/h = 1$), the green lines show a moderately confined case**

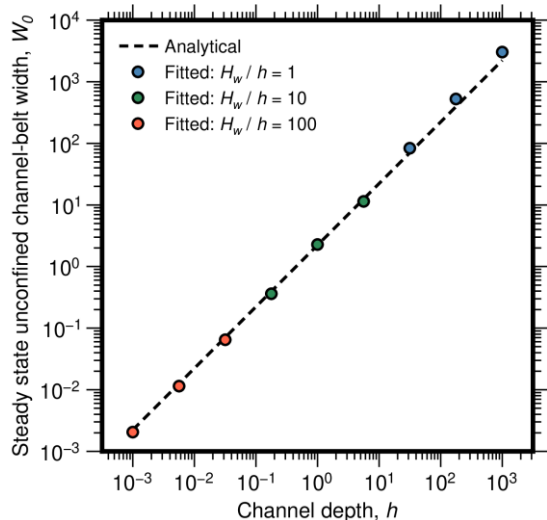
574 ($H_w/h = 10$), and the orange lines a highly confined case ($H_w/h = 100$). b), with the location density at $t = 3000$ shown
 575 in b). The dotted line on b) gives the theoretically expected normal distribution for the unconfined case (blue), the
 576 dashed line marks the law of the iterated logarithm. Colours show the unconfined case (blue, $H_w/h = 1$), a moderately
 577 confined case (green, $H_w/h = 10$), and a highly confined case (orange, $H_w/h = 100$). Flow depth $h = 1$ in all cases. c)
 578 Average width evolution with time, showing the analytical expressions for the linear (dotted lines, eq. 1), exponential
 579 (dash-dotted lines eq. 12) and drift phases (dashed lines eq. 25). Fine solid lines show the outputs from the numerical
 580 simulation and black circles show the mean widths of these simulations in bins spaced logarithmically in time.
 581 Standard errors of the means are smaller than the symbols.

582



583

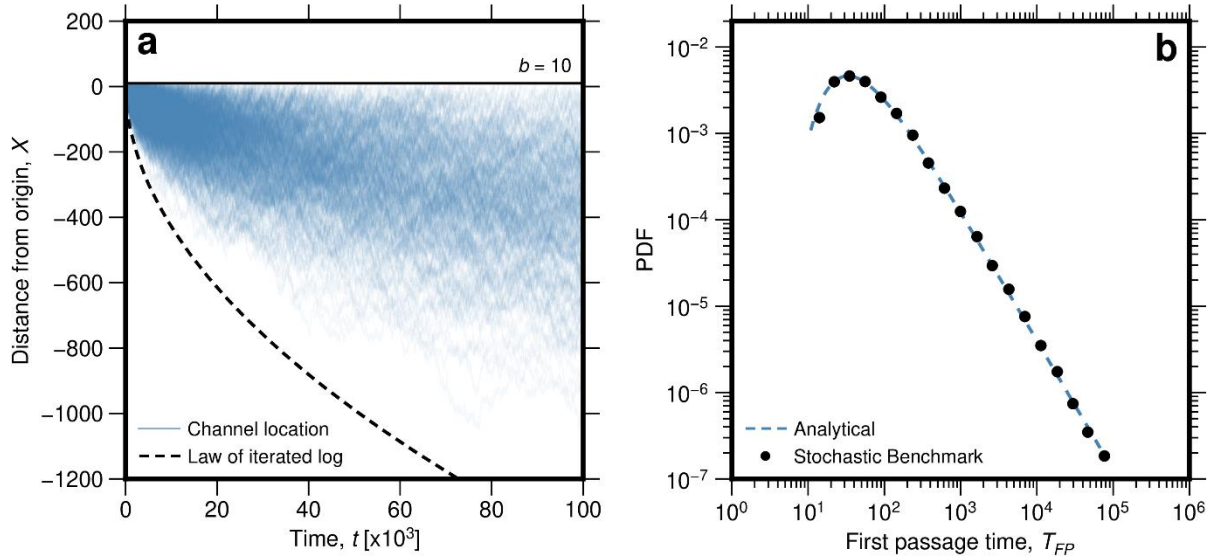
584 Fig. 3: Lateral drift velocity/speed of channel belts at constant steady state width for the drift-phase. For the
 585 calculation, channel-belt width beyond the exponential phase was fixed to the steady state width, i.e., whenever the
 586 channel widened the channel belt on one side, the width was reduced by the same amount on the other side. a) Channel
 587 location as a function of time for cases different degrees of confinement (same colour code as in Fig. 2) of H_w/h . Note
 588 that a) does not show the entire calculated trajectories; average drift velocities were measured after 10,000 steps.
 589 Average drift velocity as a function of b) Average drift velocity/speed as a function of steady width and c) lateral
 590 transport capacity from the Stochastic Benchmark numerical experiments are shown as circles, confirm the
 591 analytical predictions (dotted lines) of eq. (29) fit the numerical results well. Larger circles show simulations plotted in
 592 a) and c). Note that a) does not show the entire calculated trajectories. Average drift velocities in b) and c) were
 593 measured after 10,000 steps. c) Average drift velocity/speed as a function of lateral transport capacity with the same
 594 symbology as in b). Larger circles in b) and c) show simulations plotted in a).



595

596 Fig. 4: Verifying the value of the constant c (see eq. 30) by comparing unconfined steady state channel-belt width
 597 obtained from fits to the Stochastic Poisson Model (Fig. 1) to channel depth for varying simulations. We set channel
 598 width $W_c = 0$ and $k = 1$ for these simulations. Then, the steady state channel-belt width and flow depth should be
 599 proportional with a constant of proportionality equal to $1/c$ (eq. 4). The blue-dashed line gives the theoretically expected
 600 relationship with $c = 2.2285$ (eq. 30). The results also show that the value of c is the same for unconfined and confined
 601 channel belts.

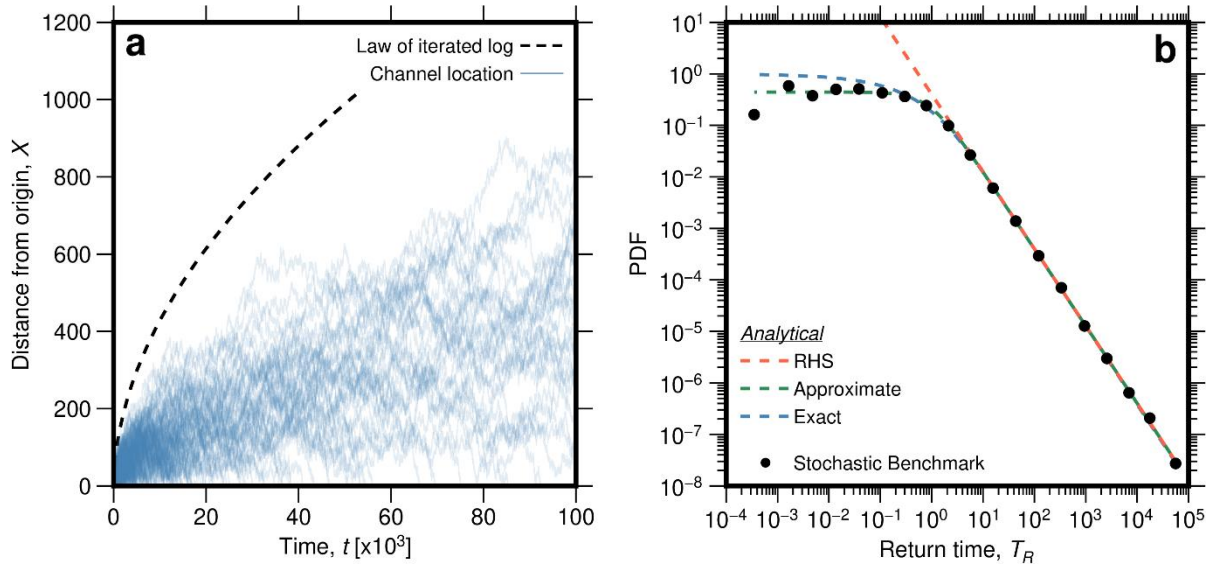
602



603

604 **Fig. 5:** The **analytical** results for the first passage distribution. a) Paths of models to investigate time distribution to
 605 reach a point a distance b from the origin (**horizontal black line**). The dashed line gives the **expectation from the**
 606 **law of the iterated logarithm** (eq. 32). In comparison to Fig. 2a, substantially longer runs in time are shown here. b) **Modelled**
 607 **first passage time distribution of the numerical experiment** **Stochastic Benchmark** (black dots show binned means) **in**
 608 **comparison to the exact analytical solution** (dotted blue line, eq. 33).

609



610

611 **Fig. 6:** The analytical results for the return time distribution, equivalent to the age distribution of sediments stored in
 612 the channel belt **and comparison to data**. a) Paths of ~~xxx~~10,000 models to investigate **the** time distribution for the return
 613 to the origin. **Once a model path reached the origin, later timesteps are it is not plotted at later timesteps**. The dashed
 614 line gives the **prediction of the return time from the law of the iterated logarithm** (eq. 32). In comparison to Fig. 2a,
 615 substantially longer runs in time are shown here. b) Modelled **return time distribution in** (circles black dots show binned
 616 **means**) **comparison compared to the exact analytical solution** (blue, eq. 34), the power law decay in the right-hand tail
 617 with an exponent of $-3/2$ (red, eq. 35). The analytical approximation (green, eq. 36) is also shown. **e) Floodplain age**
 618 **data from Everitt (1968), Skalak & Pizzuto (2010), and Huffman et al. (2022) are consistent with the $-3/2$ power law**
 619 **tail**.

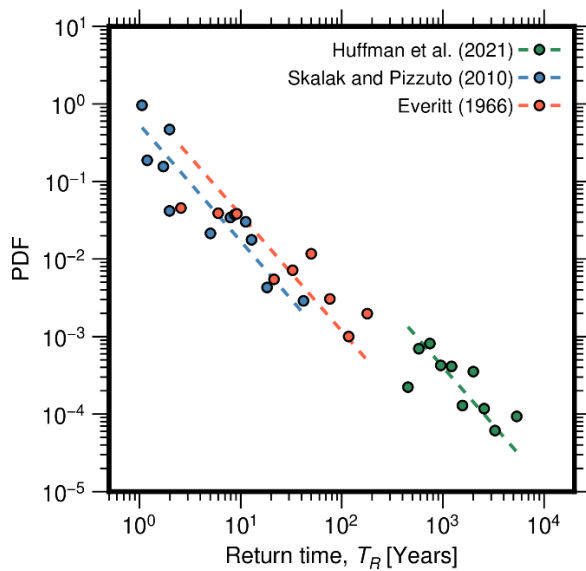
620

Table 1: Statistics for the comparison of the analytical results with the Stochastic Benchmark and the data in

Test	Equation #	Figure #	R^2
Comparison of analytical equations to the Stochastic BenchmarkSPoisson-M			
Normal distribution of channel positions		2b	0.9962550
Width increase in the exponential phase	12	2c	0.99945

Width increase in the drift phase	25	2c	0.99626
Drift velocity as function of width	29	3b	0.9999
Drift velocity as function of lateral transport capacity	29	3c	0.9999
Verification of the value of c	30	4	0.9997
First passage distribution	33	5b	0.9991
Return time distribution, exact solution	34	6b	0.9953
Return time distribution, right-hand tail	35	6b	0.9995
Return time distribution, approximate solution	36	6b	0.9980
<u>Comparison of analytical equations to data</u>			
Return time distribution, fit to Everitt (1966)	35	7	0.8434
Return time distribution, fit to Skalak & Pizzuto (2010)	35	7	0.55760.8168
Return time distribution, fit to Huffman et al. (2022)	35	7	0.55760.8168
Drift in the experiment Run 5	25	8a	0.9995
Drift in the experiment Run 7	25	8b	0.9960

621



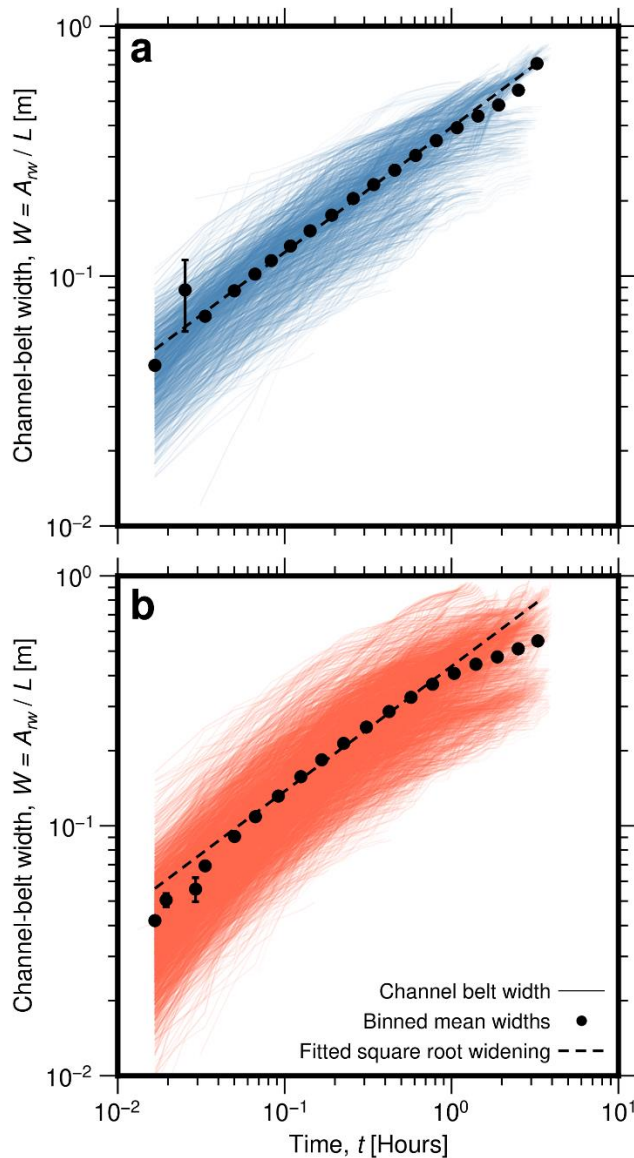
622

623

624

Fig. 7: Floodplain age data from Everitt (1968), Skalak & Pizzuto (2010), and Huffman et al. (2022) are consistent with the -3/2 power law tail (eq. 35). R^2 values for the fits are given in Table 1.

625



626

627 **Fig. 78:** Temporal evolution of the cumulative inundated area in the experiments of Bufe et al. (2016a, 2019), with data
 628 from a) Run 5 (blue) and b) Run 7 (red). Black dots give binned means, and error bars show the standard errors of the
 629 means (mostly smaller than the symbols). The dashed line is the fitted square root widening relationship with time that
 630 can be expected for the drift phase (eq. 25). **R² values for the fits are given in Table 1.**

631 5. Discussion

632 5.1 Model predictions and overview

633 Using the Poisson concept for the formation and evolution of channel belts, we derived a range of results that hold
 634 implications for fluvial geomorphology, quantitative landscape evolution studies, and river management (Table
 635 Table 42). The stochastic treatment allowed us to theoretically quantify one of the two unconstrained parameters
 636 in the model of Turowski et al. (2024). As such, apart from the factor of proportionality k in the definition of the
 637 switching timescale λ (eq. 2), all of the model parameters can be directly related to channel geometry and
 638 hydraulics. In particular, to parameterize the model, one needs measurements of flow depth h , channel width W_C ,
 639 and the lateral transport capacity q_L . The former two have been routinely measured in the field. Yet, natural river
 640 discharge changes over time, and it is currently unclear which flood size is responsible for setting the channel belt

641 in the long-term channel dynamics. The lateral transport capacity depends on discharge, sediment supply and
642 granulometry of a particular river (Bufe et al., 2019). The precise dependence is debated (e.g., Bufe et al., 2019;
643 Constantine et al., 2014; Ielpi and Lapôte, 2019; Wickert et al., 2013), and likely depends on the characteristics
644 of the particular river, for example its planform type (Greenberg et al., 2024; Nyberg et al., 2023).

645
646 Our model has been constructed assuming a single laterally migrating channel as it constructs a channel belt
647 between two avulsion events (Bridge and Leeder, 1979; Nyberg et al., 2023). Yet, many rivers are braided or
648 anastomosing, featuring multiple channels. It is not clear at the moment whether the model can also be applied to
649 those rivers. ~~There are a number of points~~A number of points can be made, though, based on generic arguments
650 and observations (Turowski et al., 2024). First, multiple channels would add a complexity to the model that is
651 beyond the first-order treatment developed here. Second, the channels in Bufe et al.'s (2016) experiments
652 frequently split into multiple channels. Nevertheless, the square root scaling expected for the drift phase can be
653 observed (Fig. 8), and observed narrowing of valleys in response to uplift closely follows the predicted
654 relationship (eq. 5) (see Turowski et al., 2024). ~~This~~These results may indicate that multiple channels lead to an
655 average rate and pattern of lateral migration similar to that of a single migrating channel. Third, Bufe et al. (2019)
656 found that q_L scales approximately linearly with water discharges in experiments featuring multiple channels. This
657 indicates that the area affected by migrating channels is independent of the detailed distribution of water between
658 single or multiple channels. How different channels interact by merging, splitting and crossing, and how this
659 affects their lateral migration speed and dynamics needs to be investigated in future work.

660
661 ~~The investigated measured age distributions are consistent with the predicted $3/2$ power law scaling. This will be~~
662 ~~discussed in detail in section 5.3. The evolution of average channel belt width in experiments shows the square~~
663 ~~root scaling with time, as expected for the drift phase (Fig. 7). The exponential approach can be fitted~~
664 ~~independently (see Bufe et al., 2019). However, the data resolution is not good enough to fit both relationships~~
665 ~~with consistent parameter values. Essentially, the resulting unconfined channel belt width W_u depends on the~~
666 ~~subjective choice of which data points to include into the fit.~~

Table 12: Overview of the analytical equations

<u>Result</u>	<u>Comment</u>	<u>Equation #</u>	<u>Equation</u>
<u>Channel lateral migration speed</u>	<u>Suggested by Bufe et al. (2019) from experimental data.</u>	<u>1</u>	$V = \frac{q_L}{H_+}$
<u>Average switching rate</u>	<u>Derived by Turowski et al. (2024).</u>	<u>2</u>	$\lambda = k \frac{q_L}{h^2}$
<u>Unconfined steady-state channel-belt width</u>	<u>Derived by Turowski et al. (2024).</u>	<u>4</u>	$W_0 = \frac{c}{k} h + W_C$
<u>Steady-state valley width</u>	<u>Includes uplift and lateral sediment supply as additional input parameters in comparison to eq. (4). Derived by Turowski et al. (2024).</u>	<u>5</u>	$W_V = \left(\frac{q_L - q_H}{U} \right) \ln \left\{ 1 + \frac{U(W_0 - W_C)}{q_L} \right\} + W_C$
<u>Exponential approach to steady state</u>	<u>The governing time scale for the unconfined case is given by eqs. (13) and (14), and for the confined case by eq. (18). Evolution equation in the exponential phase.</u>	<u>12</u>	$W(t) = W_0 - (W_0 - W_C) \exp \left\{ -\frac{t}{\tau} \right\} + W_C$
<u>Governing time scale, unconfined case</u>	<u>To be used in eq. (12).</u>	<u>13 & 14</u>	$\tau = (W_0 - W_C) \frac{H_+}{q_L} = \frac{c}{\lambda}$
<u>Governing time scale, confined case</u>	<u>To be used in eq. (12).</u>	<u>18</u>	$\tau = \frac{(W_0 - W_C)(H_W - h)}{q_L} = \left(\frac{H_W}{h} - 1 \right) \frac{c}{\lambda}$
<u>Square root widening</u>	<u>Average increase of area affected by the channel in the drift phase, after the steady state width has been reached.</u>	<u>25</u>	$W_{Drift}(t) = \sqrt{\frac{2}{k} \frac{h}{H_W} q_L t} + W_C$
<u>Average drift speed</u>	<u>Average drift speed in the drift phase, assuming the channel belt keeps a constant width.</u>	<u>29</u>	$V_{Drift} = \frac{1}{\sqrt{2}} \frac{h}{k} \frac{q_L}{H_W (W_0 - W_C)}$
<u>Channel-belt limits</u>	<u>Law of the iterated logarithm as an envelope to the area that the channel is unlikely to</u>	<u>32</u>	$X(t) = \pm 2 \frac{h}{k} \sqrt{2 \frac{\lambda t}{k} \ln \left\{ \ln \left\{ 2 \frac{\lambda t}{k} \right\} \right\}} + \frac{W_C}{2}$

	<u>leave. Only valid for unconfined channel belts.</u>		
<u>First-passage time distribution</u>	<u>Distribution of times needed to reach a point a distance b from the origin (Lévy distribution).</u>	<u>33</u>	$PDF_{FP,R}(T_{FP}) = \frac{ b }{\sqrt{2\pi \frac{h}{H_W} \frac{q_L}{k} T_{FP}^3}} \exp\left\{\frac{-b^2}{2 \frac{h}{H_W} \frac{q_L}{k} T_{FP}}\right\}$
<u>Distribution of times needed to return to the origin</u>	<u>This is equivalent to the sediment residence-time distribution, or the age distribution of sediments, assuming a single deposition and remobilisation. The integral equation does not have an analytical solution. An analytical solution for the right-hand tail is given in eq. (35), and an analytical approximation for the entire distribution in eq. (36).</u>	<u>34</u>	$PDF_{RT}(T_R)$ $= \int_0^{\frac{h}{H_W} V t} \frac{\lambda}{\frac{h}{H_W} V} \exp\left\{-\frac{\lambda}{V} \Delta x\right\} \frac{ \Delta x }{\sqrt{2\pi \frac{h}{H_W} \frac{q_L}{k} \left(T_R - \frac{\Delta x}{\frac{h}{H_W} V}\right)^3}} \exp\left\{\frac{-\Delta x^2}{2 \frac{h}{H_W} \frac{q_L}{k} \left(T_R - \frac{\Delta x}{\frac{h}{H_W} V}\right)}\right\} d\Delta x$
<u>Analytical right-hand tail of the distribution of times needed to return to the origin</u>	<u>An analytical solution for the right-hand tail of eq. (34).</u>	<u>35</u>	$PDF_{RT}(T_R \gg 0) = \frac{\lambda}{\sqrt{2\pi}} \left(\frac{h}{H_W} \lambda T_R\right)^{-3/2}$
<u>Analytical approximation for the distribution of times needed to return to the origin</u>	<u>Analytical approximation for eq. (34).</u>	<u>36</u>	$PDF_{RT}(T_R) \approx \frac{1}{\sqrt{2\pi}} \frac{h}{H_W} \frac{a\lambda}{1 + a \left(\frac{h}{H_W} \lambda T_R\right)^{3/2}}$ $a = \left(\frac{3}{2}\right)^3 \left(\frac{3}{2\pi}\right)^{3/2} = 1.1135$
<u>Value for time scaling constant c.</u>	<u>The constant relates the average switching rate λ to the effective switching time ΔT (see eq. 3).</u>	<u>30</u>	$c = \frac{1}{\sqrt{2} \frac{V_{Drift}}{V}} = 2.2285$

670 **Table 1: Overview of the analytical equations**

Result	Comment	Equation #
Channel lateral migration speed	Suggested by Bufe et al. (2019) from experimental data.	1
Average switching rate	Derived by Turowski et al. (2024).	2
Unconfined steady state channel belt width	Derived by Turowski et al. (2024).	4
Steady state valley width	Includes uplift and lateral sediment supply as additional input parameters in comparison to eq. (4). Derived by Turowski et al. (2024).	5
Exponential approach to steady state	The governing time scale for the unconfined case is given by eqs. (13) and (14), and for the confined case by eq. (18).	12
Square root widening	Average increase of area affected by the channel in the drift phase, after the steady state width has been reached.	25
Average drift speed	Average drift speed in the drift phase, assuming the channel belt keeps a constant width.	29
Channel belt limits	Law of the iterated logarithm as an envelope to the area that the channel is unlikely to leave. Only valid for unconfined channel belts.	32
First passage time distribution	Distribution of times needed to reach a point a distance b from the origin.	33
Distribution of times needed to return to the origin	This is equivalent to the sediment residence time distribution, or the age distribution of sediments, assuming a single deposition and remobilisation. The integral equation does not have an analytical solution. An analytical solution for the right hand tail is given in eq. (35), and an analytical approximation for the entire distribution in eq. (36).	34

5.2 The effect of uplift

In our model ~~derivations~~, we have not explicitly considered the role of uplift or net incision on the channel-belt width. Uplift increases the bank height encountered by the channel in lateral motion (eq. 1) and thereby slows it down. Turowski et al. (2024) included uplift in their steady state valley-width model and demonstrated that a competition between uplift and lateral

mobility of the channel, described by the lateral transport capacity, determines the final width of the valley. Yet, the inclusion of uplift in the [stochastic treatment](#) [Stochastic Poisson Model](#) developed herein would introduce considerable [complexities](#) [complexity](#) into the equations. It seems unlikely that analytical solutions are possible. Here, we suggest a simple approach to circumvent this problem. We [equate-use equations \(1\) to \(5\) and \(459\)](#) to define an effective lateral migration speed \overline{V}_U [LT⁻¹] in an uplifted area

$$W = \frac{c\overline{V}_U}{\lambda} + W_C = \frac{q_L}{U} \ln \left\{ 1 + \frac{U(W_0 - W_C)}{q_L} \right\} + W_C. \quad (37)$$

Solving for \overline{V}_U , this yields

$$\overline{V}_U = \frac{kV^2}{cU} \ln \left\{ 1 + \frac{U(W_0 - W_C)}{q_L} \right\} \quad (38)$$

We thus obtain an effective variance

$$\begin{aligned} VAR &= \frac{2}{k} \frac{h}{H_W} \frac{\overline{V}_U^2}{\lambda} t = \frac{2}{k} \left(\frac{k}{c} \right)^2 \frac{h}{H_W} \frac{V^4 t}{U^2 \lambda} \ln^2 \left\{ 1 + \frac{U(W_0 - W_C)}{q_L} \right\} \\ &2 \left(\frac{k}{c} \right)^2 \frac{h}{H_W} \frac{q_L^2}{(W_0 - W_C) U^2} q_L t \ln^2 \left\{ 1 + \frac{U(W_0 - W_C)}{q_L} \right\} \end{aligned} \quad (39)$$

Equation (39) can be used in equation (19) for the drift to account for uplift. Other results also have to be updated accordingly. The approach outlined above needs to be benchmarked with numerical simulations, [field or experimental data](#).

5.3 First-passage and floodplain age distributions

The Lévy distribution (eq. 33) describes the time needed until the channel moves a particular distance away from its starting location. When integrated to infinity, the distribution has an infinite mean and variance. Nevertheless, [under the assumption of constant or effective flow conditions](#), it could be used, for example, for assessing the risk of the destruction of a building near a river channel within a given timespan.

Lateral river dynamics determine the reworking of sediment in the floodplain, and, therefore, determine storage times and sediment ages (e.g., Bradley & Tucker, 2013). This has, for example, implications for chemical alteration of floodplain sediments, such as chemical weathering and organic carbon oxidation (e.g., [Scheingross et al., 2021](#); Repasch et al., 2020; Torres et al., 2017). It has frequently been found [that](#) residence time distributions are highly skewed, and that the mean residence time of sediment is much larger than their median residence time (e.g., Carretier et al., 2020; Pizzuto et al., 2017). Measurements of the distribution of floodplain ages have yielded a variety of contrasting behaviour (Pizzuto et al., 2017). The right-hand tail of the distribution of field data has been characterized both by an exponential (e.g., Huffman et al., 2022;

705 Lancaster & Casebeer, 2007) and by a power law function (e.g., Bradley & Tucker, 2013; Pizzuto et al., 2017), in the latter case with exponents ranging from about -0.7 to about -1.53/21.5 (e.g., ~~Everitt, 1968~~; Lancaster et al., 2010; Pizzuto et al., 2017; Skalak & Pizzuto, 2010). Pizzuto et al. (2017) used a random walk to model the stochastic downstream motion of sediment to predict power-law travel-time distributions with exponents that decrease with increasing length of the river system.

710 Bradley & Tucker (2013) suggested that the Lévy distribution is suitable to model the distribution of floodplain ages. Analogous to our result for the age distribution (eq. 34), the Lévy distribution features a power-law right-hand tail with a scaling exponent of -1.53/2 (eq. 33). However, it strongly underpredicted the likelihood of small ages as generated by Bradley & Tucker's (2013) numerical model. The Lévy distribution has been derived for the time of the first passage of a point a pre-selected distance from the origin (eq. 33), and this distance cannot be equal to zero in the assumptions of the derivation. It therefore is not the correct distribution for the times to return to the origin. We derived a probability distribution for the time to return to the origin (eq. 34). The right-hand tail of the residence time distribution (eq. 35) exhibits the same scaling of the right-hand tail of the Lévy distribution (eq. 33), a power law with an exponent of -1.53/2 (Fig. 6b). In fact, this scaling is valid for any symmetric random walk, and should be independent of the precise assumptions used to set up such a random walk. It implies that the return-time distribution has both an infinite mean and standard deviation when integrated to infinity, similar to the distribution of first passage. This result implies that the mean age measured for a sediment body within a channel belt does not converge to a fixed value, but depends on the time since the onset of fluvial activity, no matter how long ago this onset occurred. The result implies that statements on the age of sediment in floodplains, or their chemical alteration, always have to be made with respect to the total age of the floodplain. A long-term average at steady state is never achieved. Further, it implies that some fluvial deposits are likely to survive for long times, storing information about the floodplain evolution and the history of river systems (cf. Carretier et al., 2020). The increase of the mean sediment residence time \bar{T}_R can be obtained by integrating the age distribution (eq. 34) multiplied with time, as in the integration for the mean. We can obtain the limit behaviour for old river systems by integrating over eq. (35)

$$\bar{T}_R(t) = \int_0^{T_A} \frac{\lambda}{\sqrt{2\pi}} \left(\frac{h}{H_W} \lambda t \right)^{-3/2} t dt = \sqrt{\frac{2}{\pi}} \left(\frac{H_W}{h} \right)^3 \frac{T_A}{\lambda}. \quad (40)$$

730 Here, T_A is the time since the formation of the channel belt. The mean residence time thus increases with the square root of time in this limit. In combination with eq. (35), eq. (40) can be used to estimate the age of a channel belt from sediment age data.

735 Our prediction of the -1.53/2-scaling exponent in the age distribution (eqs. 34, 35) does align with some, but not all of the measurements reported in the literature (cf. Pizzuto et al., 2017). It is consistent with the data of Everitt (1966), Skalak & Pizzuto (2010), and Huffman et al. (2022) that we digitised for the present study (Fig. 6e7), but not with the datasets reported

for example by Lancaster et al. (2010). ~~For our comparison, we selected data sets that, on first glance, comply with the assumptions underlying our model~~Stochastic Poisson Model. ~~Our~~The model framework is strictly valid only for processes that can be modelled by a lateral random walk ~~of a single channel~~ in an infinite domain. ~~As such, we expect it to apply to single-thread channels without major tributaries that are undisturbed by processes other than fluvial erosion and deposition. We expect that~~Further, the ~~-1.53/2~~-scaling applies to channels that are short enough such that sediment, once it is eroded, is not redeposited within the system, but evacuated downstream. Alternatively, ~~if~~the scaling could apply ~~to data measured with~~for dating methods where the date is reset after remobilization of sediment, for example optically stimulated luminescence (e.g., Madsen & Murray, 2009). Multiple episodes of deposition and erosion within the same system yields a power-law tail with an exponent that is dependent on the system size (Pizzuto et al., 2017). This exponent should, generally, be smaller than ~~-3/2+5~~, because re-deposition will increase the relative fraction of old sediment. Even in short systems, the derived age distribution (eq. 34) cannot be expected to be universally applicable. We expect that channels confined in a narrow valley, or those in which processes other than lateral channel migration can deposit, evacuate or mobilize sediment, show different scaling behaviour. For example, ~~Cedar Creek and Golden Ridge Creek, both~~the channels ~~studied by Lancaster and Casebeer (2007) and Lancaster et al. (2010) are located~~ in confined valleys where debris flows regularly supply and mobilize sediment ~~(Lancaster et al., 2010), and~~ exhibit age distributions with power-law scaling exponents of the order of -0.7. In narrowly confined settings, sediment deposition and erosion may not be adequately described by a random walk. Further, ~~the disturbance of fluvial deposits and~~ lateral sediment supply ~~by~~due to debris flows or hillslope processes may have a large effect on the age distribution.

5.4 Parameter estimation and further tests

~~Two of the parameters in the model need further scrutiny. First, the hydraulic and geometric controls on the lateral transport capacity q_L are not fully resolved. This parameter can, in principle, be investigated in experiments (e.g., Bufe et al., 2019; Wickert et al., 2013) and nature (e.g., Constantine et al., 2014; Greenberg & Ganti, 2024; Ielpi & Lapôtre, 2019). Bufe et al. (2019) presented a discussion and synthesis of the available evidence from experimental and natural channels, as well as a dimensionless analysis of potential control parameters. We will not further discuss this parameter here. Second,~~the model contains a single dimensionless scaling factor, k , which is the factor of proportionality of the rate of switches of direction of motion of the channel λ and the ratio of the lateral transport capacity q_L and the square of the flow depth h (eq. 2). This parameter sets the unconfined channel-belt width (eq. 4). Two strategies for measuring this parameter appear from our results. First, exploiting eq. (2) relies on direct measurements of the switching rate, as well as flow depth and q_L . The switching rate λ can also be measured from the age distribution of sediment (eq. 41). Second, the width of the channel belt can be related to flow depth and channel width using eq. (4). Both approaches seem more promising in an experimental setting than in nature, because the necessary parameters can be either controlled or measured directly. In the field, it may be possible to obtain suitable data, for example, from time series of orthophotos of river reaches (e.g., Nyberg et al., 2023; Greenberg & Ganti, 2024;

Greenberg et al., 2024) in combination with gauging data. Testing for the consistency of both approaches would be a strong
770 method to falsify or validate the model.

Our model is constructed at the reach scale of the channel and does not include detailed descriptions of fluvial processes. Yet, it should be possible to relate it to process-based models. Here, we make a tentative relation to models of meandering channels, which are available at different degrees of complexity (e.g., Edwards & Smith, 2002; Ikeda et al., 1981). Camporeale et al.
775 (2005) studied models of meandering rivers at increasing levels of hydraulic detail. They concluded that the steady state statistics of the meander belt are determined by only two parameters, regardless of the complexity of the model. These are a length scale D_0 [L] proportional to the ratio of flow depth and the friction coefficient ~~of the~~for open channel flow C_f

$$D_0 = \frac{h}{2C_f}, \quad (41)$$

780 and a time scale T_0 [T], given by

$$T_0 = \frac{D_0^2}{W_c U_f E}. \quad (42)$$

Here, U_f [LT^{-1}] is the mean streamwise flow speed and E [-] a dimensionless bank erodibility coefficient. Using their model considerations together with field observation, Camporeale et al. (2005) found that the meander belt width W_{MB} can be
785 described by

$$W_{MB} = \alpha D_0 = \frac{\alpha h}{2C_f}. \quad (43)$$

Here, α [-] is a dimensionless proportionality coefficient with a value of 40 to 50. We can use eqs. (41) to (43) to make a tentative connection between our landscape-scale random walk model, and the reach-scale meandering models. First, we
790 note both models suggest that channel-belt width is proportional to flow depth (see eq. 4). Comparing eqs. (4) and (43), we suggest that k_0 scales as

$$k_0 = \frac{c}{k} = \frac{\alpha}{2C_f}. \quad (44)$$

As such, we expect k to scale with the friction coefficient. Assuming $C_f = 0.05$ and $\alpha = 50$ (see Camporeale et al., 2005), we
795 obtain $k = 0.0045$ and $k_0 = 500$. Second, we can assume that the governing time scale τ (eqs. 13, 14) is proportional to T_0 . Equating [equationss-](#) (14) and (42), and substituting [equationss-](#) (2), (41), and (43), we obtain

$$\frac{c}{\lambda} = \frac{ch^2}{kq_L} = \frac{\alpha h^2}{2C_f q_L} = \frac{D_0^2}{W_c U_f E} = \left(\frac{h}{2C_f}\right)^2 \frac{1}{W_c U_f E}. \quad (45)$$

800 Equation (45) can be solved for q_L to give

$$q_L = 2\alpha C_f W_c U_f E. \quad (46)$$

805 We can obtain some of the parameter values from the data used in this study. From fits to the [floodplain](#) age distributions, we obtain $\lambda = 0.12 \text{ yr}^{-1}$ (Everitt, 1966), $\lambda = 0.55 \text{ yr}^{-1}$ (Skalak & Pizzuto, 2010), and $\lambda = 0.00097 \text{ yr}^{-1}$ (Huffmann et al., 2022). Note that we assumed an unconfined channel belt for determining λ , i.e., we set $H_w = h$. In case of confinement, the estimates change with the ratio of the flow depth and the height of the confining walls (eq. 35). The numbers for the mean rate of switching seem plausible, varying from biannual switches (Skalak & Pizzuto, 2010) to once in a thousand years (Huffmann et al., 2022). The estimates should be further refined with detailed case studies.

810 5.5 Beyond the evolution of single cross sections

In the [Stochastic Poisson Model](#) developed herein, we concentrated on a single cross section, making the assumption that each cross section evolves independently of those upstream and downstream. This assumption is ~~unlikely~~ to [be a simplification when applied in real river systems](#). In particular, we can expect that a channel that locally moves laterally far from the channel position upstream and downstream is pulled back towards the center. That is, a channel within a particular cross section of the valley is less likely to further migrate laterally into the same direction if within the cross sections upstream and downstream the channel has not migrated as far, or is moving in the opposite direction. This effect can be included into the model by modulating the probability of switching direction λ within the cross section of interest depending on the position of its channel with respect to the entire river system or to the cross sections immediately upstream and downstream. We suggest that the behaviour can be modelled by an Ornstein-Uhlenbeck process (e.g., Uhlenbeck & Ornstein, 1930), similar to the Langevin equation (Langevin, 1908), which includes a term that increases the probability to move back towards the origin as a function of the distance from it. It is beyond the scope of the present contribution to develop such a model. We expect that the suggested approach will yield a Gaussian distribution of channel positions, with similar results to those derived herein, but additional dimensionless scaling factors in the variances.

6. Conclusion

825 We have described the temporal evolution of [unconfined and confined](#) channel-belt width in the framework of a random walk. [The temporal evolution can be described in three phases, which are associated with distinct timescales. First, channel belts grow linearly before the channel switches direction. Then, the channel-belt width increases exponentially until the steady state](#)

width is achieved. Finally, the channel belt enters the drift phase, where it grows on average with the square root of time. Using the mathematics of random walks, we derived a range of other results, including the limits of the channel belt (law of the iterated logarithm), the distribution of times to arrive at a particular distance from the origin (first passage distribution), and the distribution of times until the channel returns to its origin, which is equivalent to the distribution of sediment ages within the channel belt. All results directly connect to hydraulic parameters such as flow depth, channel width, and the lateral transport capacity, and the model contains a single free parameter that needs to be calibrated on data. To validate the Stochastic Poisson Model, model predictions were compared to numerical simulations of channel-belt evolution, field data of floodplain ages, and analog experiments. The comparisons strongly support the basic assumption that channel belt development can be described by a random walk. The model can in principle be used for forward predictions in the context of river management, flood hazard mitigation, and stream restoration, or for inverting fluvial strata for paleo-hydraulic conditions. Further, Our work provides a theoretical framework to interpret observational data related to fluvial landscapes evolution, nutrient cycling, and channel-floodplain interactions. The predicted scaling exponent for the age distribution of floodplain sediments is consistent with observations from streams that were selected to closely align with the assumption made in the model. In the experimental data (Bufe et al., 2016a,b, 2019), average widening proceeds with the square root of time, as expected for the drift phase. Recent global datasets on channel belts derived by automatic processing of remote sensing data (e.g., Greenberg & Ganti, 2024, Greenberg et al., 2024; Nyberg et al., 2023) provide opportunities for comprehensive testing of the model. We have provided a range of analytical results (Table 42) that allow easy comparison of theory and data. These can also be directly implemented into landscape evolution models without major numerical costs, allowing a more comprehensive and realistic depiction of landscape dynamics. The Stochastic Poisson Model can in principle be used for forward predictions in the context of river management, flood hazard mitigation, and stream restoration. In addition, our work provides a theoretical framework to interpret observational data related to fluvial landscapes evolution, nutrient cycling, and for inverting fluvial strata for paleo-hydraulic conditions. In summary, Further, all model parameters of the Stochastic Poisson Model have a direct physical interpretation, and there is a single free, dimensionless scaling parameter that needs to be informed by data. As such, our approach can bridge across spatio-temporal scales and connect landscape-scale models with those operating on the process scale.

<i>Symbol</i>	<i>Parameter</i>	<i>First appears in eq.</i>
α	Dimensionless proportionality coefficient with a value of 40 to 50 [-]	42
λ	Rate parameter of the Poisson process describing the switch in the direction of river motion [T ⁻¹]	2
τ	Governing timescale for the transient approach to a steady state [T]	12
a	Dimensionless constant approximately equal to 1.1135 [-]	36
b	Distance of an point of interest from the river channel at $t = 0$ [L]	33
c	dimensionless constant approximately equal to 2.2285 [-]	3
C_f	Open channel flow friction coefficient [-]	40
D_0	Characteristic length scale of meander belts [L]	40
E	Dimensionless bank erodibility coefficient [-]	41
h	Flow depth [L]	2
H_+	Height of the river bank in the direction of river motion [L]	1
H_w	Height of the walls confining the channel belt [L]	17
k	Dimensionless constant of order 10^{-2} to 10^{-3} [-]	2
k_0	Dimensionless constant of order 10^2 , defined by c/k [-]	4
n	Number of stochastic events, generally used for the number of steps in the random walk [-]	6
m	Number of pairs of steps in the random walk, generally defined as $n/2$ [-]	
q_H	Rate of lateral sediment supply from hillslopes or valley walls per channel length [L ² T ⁻¹]	5
q_L	Lateral-transport capacity, i.e. the amount of sediment that the channel can move by lateral erosion per unit channel length per unit time [L ² T ⁻¹]	1
P	Fraction of time that a river spends at any of its channel belt margin [-]	9
$P_{confined}$	Fraction of time that a river spends at any of its channel belt margins for a confined belt [-]	15
S	Dimensionless envelope distance for the channel belt in the law of the iterated logarithm [-]	31
t	Time [T]	4
t^*	Dimensionless time [-]	31
Δt	Average switching timescale in the Poisson process [T]	6
T_0	Characteristic time scale of meander belts [T]	41
ΔT	The characteristic length of time the river moves on average in the same direction [T]	3
T_A	Time since the formation of the channel belt; age of the channel belt [T]	40

T_{FP}	First passage time, first point in time when the channel reaches at a point of interest located a distance b from the channel at $t = 0$ [T]	33
T_R	Time needed to return to the origin for the first time [T]	34
\bar{T}_R	Mean residence time of sediment [T]	
T_{SS}	Time at which the steady state width is reached [T]	27
T_W	Waiting times between events in a Poisson process [T]	7
U	Uplift rate [$L T^{-1}$]	5
U_f	Mean streamwise flow speed [$L T^{-1}$]	41
v	Lateral speed of the river as it reaches valley-floor margins, i.e. wall toes [$L T^{-1}$]	15
V	Lateral migration speed, i.e. the speed of river migrating back and forth across the valley floor [$L T^{-1}$]	1
\bar{V}	Average lateral channel migration speed in a confined channel belt [$L T^{-1}$]	23
V_{Drift}	Average lateral speed of a channel belt with constant width during the drift phase [$L T^{-1}$]	29
VAR_{CCB}	Variance of a confined channel-belt width [L^2]	24
VAR_{UCB}	Variance of an unconfined channel-belt width [L^2]	19
W	Channel-belt width [L]	5
W_c	River channel width [L]	4
W_{Drift}	Width of channel belt in the drift phase [L]	19
W_{MB}	Width of a meander belt [L]	42
W_V	Valley floor width [L]	5
W_0	Unconfined channel-belt width [L]	4
Δx	Distance travelled by the channel before switching direction for the first time [L]	34
X	Envelope distance for the channel belt in the law of the iterated logarithm, dimensional version of S [L]	32
X_{Drift}	Average distance drifted in the drift phase [L]	26

Data availability

Raw data for the experimental datasets are stored on the SEAD repository of Bufe et al. (2016b) with the identifier
860 <http://dx.doi.org/10.5967/M0CF9N3H>. Derived quantities have been compiled from Bufe et al. (2016a,b) and Bufe et al. (2019). Sediment age data were digitised from the respective publications. Scripts used to generate Figures 2-7 are available in the publication by M^cNab (2024) with identifier <https://doi.org/10.5281/zenodo.12806574>.

Competing interests

865 At least one of the (co-)authors is a member of the editorial board of Earth Surface Dynamics. The authors ~~also~~ have no other competing interests to declare.

Author contributions

JMT, AB and ST conceived this study. JMT designed and developed the theoretical approach and derived the equations with
870 input of FM and AB, and wrote the paper. FM wrote the scripts for the ~~numerical model~~ [Stochastic Benchmark](#) and generated data figures. ST made illustrations. FM and AB developed and conducted the analysis of the experimental data. All authors contributed to data analysis, discussion, ~~and~~ writing, [and revisions](#).

Acknowledgments

875 Sophie Katzung implemented a first numerical realisation of the Poisson model and explored some of the implications of the random walk formulation during an internship [with JMT](#). FM was supported by ERC Consolidator Grant #863490 GyroSCoPe to Taylor Schildgen. [We thank two anonymous reviewers for their constructive comments on a previous version of the manuscript.](#)

References

- 880 Allen, J. R. L. ~~(1978)~~: Studies in fluvial sedimentation: An exploratory quantitative model for the architecture of avulsion-controlled alluvial suites. *Sedimentary Geology*, 21(2), 129–147. [https://doi.org/10.1016/0037-0738\(78\)90002-7](https://doi.org/10.1016/0037-0738(78)90002-7), 1978.
- Anderson, M. P., Aiken, J. S., Webb, E. K., & Mickelson, D. M.: Sedimentology and hydrogeology of two braided stream deposits. *Sedimentary Geology*, 129(3-4), 187–199. [https://doi.org/10.1016/S0037-0738\(99\)00015-9](https://doi.org/10.1016/S0037-0738(99)00015-9), 1999.
- Badoux, A., Andres, N., & Turowski, J. M.: Damage costs due to bedload transport processes in Switzerland, *Natural Hazards and Earth System Science*, 14, 279-294, <https://doi.org/10.5194/nhess-14-279-2014>, 2014.
- 885 Baley, P. B.: The flood pulse advantage and the restoration of river-floodplain systems, *Regulated Rivers: Research & Management*, 6, 75-86, <https://doi.org/10.1002/rrr.3450060203>, 1991.
- Bertoldi, W., Zanoni, L., & Tubino, M. ~~(2009)~~: Planform dynamics of braided streams. *Earth Surface Processes and Landforms*, 34(4), 547–557, <https://doi.org/10.1002/esp.1755>, 2009.

- 890 [Best, J.: Anthropogenic stresses on the world's big rivers, *Nature Geoscience*, 12, 7-21, https://doi.org/10.1038/s41561-018-0262-x, 2019.](https://doi.org/10.1038/s41561-018-0262-x)
- Blum, M., Martin, J., Milliken, K., & Garvin, M.: Paleovalley systems: Insights from Quaternary analogs and experiments. *Earth-Science Reviews*, 116, 128–169. <https://doi.org/10.1016/j.earscirev.2012.09.003>, 2013.
- Bradley, D. N., & Tucker, G. E.: The storage time, age, and erosion hazard of laterally accreted sediment on the floodplain of
895 a simulated meandering river, *Journal of Geophysical Research*, 118, 1308-1319, <https://doi.org/10.1002/jgrf.20083>, 2013.
- Bridge, J. S.: Characterization of fluvial hydrocarbon reservoirs and aquifers: problems and solutions. *Latin American Journal of Sedimentology and Basin Analysis*, 8(2), 87–114, 2001.
- Bridge, J. S., & Leeder, M. R.: A simulation model of alluvial stratigraphy, *Sedimentology*, 26, 617-644, <https://doi.org/10.1111/j.1365-3091.1979.tb00935.x>, 1979.
- 900 Bufo, A., Burbank, D. W., & Paola, C.: Fold erosion by an antecedent river, University of Michigan ARC Repository, 340 <http://dx.doi.org/10.5967/M0CF9N3H>, 2016b.
- Bufo, A., Paola, C., & Burbank, D. W.: Fluvial bevelling of topography controlled by lateral channel mobility and uplift rate, *Nature Geoscience*, 9(9), 706-710, <https://doi.org/10.1038/ngeo2773>, 2016a.
- Bufo, A., Turowski, J. M., Burbank, D. W., Paola, C., Wickert, A. D., & Tofelde, S.: Controls on the lateral channel-migration
905 rate of braided channel systems in coarse non-cohesive sediment: *Earth Surface Processes and Landforms*, 44(14), 2823-345 2836, <https://doi.org/10.1002/esp.4710>, 2019.
- Carretier, S., Guerit, L., Harries, R., Regard, V., Maffre, P., & Bonnet, S.: The distribution of sediment residence times at the foot of mountains and its implications for proxies recorded in sedimentary basins, *Earth and Planetary Science Letters*, 546, 116448, <https://doi.org/10.1016/j.epsl.2020.116448>, 2020.
- 910 Constantine, J. A., Dunne, T., Ahmed, J., Legleiter, C., & Lazarus, E. D.: Sediment supply as a driver of river meandering and floodplain evolution in the Amazon Basin. *Nature Geoscience*, 7(12), 899–903. <https://doi.org/10.1038/ngeo2282>, 2014.
- [Edwards, B. F. and Smith, D. H.: River meandering dynamics, *Phys. Rev. E*, 65, 046303, https://doi.org/10.1103/PhysRevE.65.046303, 2002.](https://doi.org/10.1103/PhysRevE.65.046303)
- Egozi, R., & Ashmore, P.: Experimental analysis of braided channel pattern response to increased discharge. *Journal of*
915 *Geophysical Research*, 114, F02012. <https://doi.org/10.1029/2008JF001099>, 2009.
- Everitt, B.L.: Use of the cottonwood in an investigation of the recent history of a flood plain, *Am. J. Sci.*, 266, 417-439, 1968.
- Fotherby, L. M.: Valley confinement as a factor of braided river pattern for the Platte River, *Geomorphology*, 103, 562-576, <https://doi.org/10.1016/j.geomorph.2008.08.001>, 2009.
- Greenberg, E., & Ganti V.: The pace of global river meandering influenced by fluvial sediment supply, *Earth Planet. Sci. Lett.*,
920 634, 118674, <https://doi.org/10.1016/j.epsl.2024.118674>, 2024.
- Greenberg, E., Chadwick, A. J., Li, G. K., & Ganti V.: Quantifying channel mobility and floodplain reworking timescales across river planform morphologies, *Geophys. Res. Lett.*, 51, e2024GL108537, <https://doi.org/10.1029/2024GL108537>, 2024.

- Junk, W. J., Bayley, P. B., & Sparks, R. E.: The flood pulse concept in river-floodplain systems, p. 110-127 in D. P. Dodge
925 (Ed.), Proceedings of the International Large River Symposium. Can. Spec. Publ. Fish. Aquat. Sci. 106, 1989.
- Hajek, E. A., & Straub, K. M.: Autogenic sedimentation in clastic stratigraphy. Annual Review of Earth and Planetary
Sciences, 45(1), 681–709. <https://doi.org/10.1146/annurev-earth-063016-015935>, 2017.
- Hancock, G. S., & Anderson, R. S.: Numerical modeling of fluvial strath-terrace formation in response to oscillating climate.
Bulletin of the Geological Society of America, 114(9), 1131–1142. <https://doi.org/10.1130/0016-350>
930 7606(2002)114<1131:NMOFST>2.0.CO, 2002.
- Howard, A. D.: Modelling Channel Evolution and Floodplain Morphology, In M. G. Anderson, D. E. Walling, & P. E. Bates
(Eds.), Floodplain processes (pp. 15–62). Chichester: John Wiley and Sons, Ltd., 1996.
- Huffman, M. E., Pizzuto, J. E., Trampush, S. M., Moody, J. A., Schook, D. M., Gray, H. J., & Shannon, A. M.: Floodplain
sediment storage timescales of the laterally confined meandering Powder River, USA, J. Geophys. Res., 127,
935 e2021JF006313, <https://doi.org/10.1029/2021JF006313>, 2022.
- Ielpi, A., & Lapôtre, M. G. A.: A tenfold slowdown in river meander migration driven by plant life, Nature Geoscience, 13,
82-86, <https://doi.org/10.1038/s41561-019-0491-7>, 2019.
- [Ikeda, S., Parker, G., and Sawai, K.: Bend theory of river meanders. Part 1. Linear development, J. Fluid Mech., 112, 363–
377, https://doi.org/10.1017/S0022112081000451, 1981.](https://doi.org/10.1017/S0022112081000451)
- 940 Jonell, T. N., Owen, L. A., Carter, A., Schwenniger, J.-L., & Clift, P. D.: Quantifying episodic erosion and transient storage
on the western margin of the Tibetan Plateau, upper Indus River. Quaternary Research, 89, 281-306,
<https://dx.doi.org/10.1017/qua.2017.92>, 2018.
- Kolmogoroff, A.: Über das Gesetz des iterierten Logarithmus, Mathematische Annalen, 101, 126–135, 1929.
- Lancaster, S. T., & Casebeer, N. E.: Sediment storage and evacuation in headwater valleys at the transition between debris-
945 flow and fluvial processes, Geology, 35(11), 1027-1030, <https://dx.doi.org/10.1130/G239365A.1>, 2007.
- Lancaster, S. T., Underwood, E. F., & Frueh, W. T.: Sediment reservoirs at mountain stream confluences: dynamics and effects
of tributaries dominated by debris-flow and fluvial processes, Geol. Soc. Am. Bull., 122, 1775-1786,
<https://dx.doi.org/10.1130/B30175.1>, 2010.
- Langevin, M. P.: On the theory of Brownian motion, C. R. Acad. Sci. (Paris) 146, 530–533, 1908.
- 950 Lawler, G. F., & Limic, V.: Random Walk: A modern introduction, Cambridge University Press, ISBN 9780511750854,
<https://doi.org/10.1017/CBO9780511750854>, 2010.
- Limaye, A. B. S.: How do braided rivers grow channel belts? Journal of Geophysical Research: Earth Surface, 125, 1–24.
<https://doi.org/10.1029/2020JF005570>, 2020.
- Maddy, D., Bridgland, D., & Westaway, R.: Uplift-driven valley incision and climate-controlled river terrace development in
955 the Thames Valley, UK. Quaternary International, 79(1), 23–36. [https://doi.org/10.1016/s1040-6182\(00\)00120-8](https://doi.org/10.1016/s1040-6182(00)00120-8), 2001.
- Madsen, A. T., & Murray, A. S.: Optically stimulated luminescence dating of young sediments: A review, Geomorphology,
109, 3–16. <https://doi.org/10.1016/j.geomorph.2008.08.020>, 2009.

- Malatesta, L. C., Prancevic, J. P., & Avouac, J. P.: Autogenic entrenchment patterns and terraces due to coupling with lateral erosion in incising alluvial channels. *Journal of Geophysical Research: Earth Surface*, 122, 335–355. <https://doi.org/10.1002/2015JF003797>, 2017.
- 960 <https://doi.org/10.1002/2015JF003797>, 2017.
- [Marr, J. G., Swenson, J. B., Paola, C., & Voller, V. R.: A two-diffusion model of fluvial stratigraphy in closed depositional basins, *Basin Research*, 12, 381-398, <https://doi.org/10.1111/j.1365-2117.2000.00134.x>, 2000.](https://doi.org/10.1002/2015JF003797)
- Martin, J., Cantelli, A., Paola, C., Blum, M., & Wolinsky, M.: Quantitative modeling of the evolution and geometry of incised valleys. *Journal of Sedimentary Research*, 81(1), 64–79. <https://doi.org/10.2110/jsr.2011.5>, 2011.
- 965 May, C., Roering, J., Eaton, L. S., & Burnett, K. M.: Controls on valley width in mountainous landscapes: The role of 360
landsliding and implications for salmonid habitat. *Geology*, 41(4), 503–506. <https://doi.org/10.1130/G33979.1>, 2013.
- McNab, F.: Supplement to: "Width evolution of channel belts as a random walk" by Turowski et al., Version 12, Zenodo, <https://doi.org/10.5281/zenodo.1336459410.5281/zenodo.12806574>, 2024.
- Meitzen, K. M., Kupfer, J. A., & Gao, P.: Modeling hydrologic connectivity and virtual fish movement across a large
970 Southeastern floodplain, USA, *Aquatic Sciences*, 80(5), <https://doi.org/10.1007/s00027-017-0555-y>, 2018.
- Miller, A. J.: Valley morphology and boundary conditions influencing spatial patterns of flood flow. In: Costa, J. E., Miller, A. J., Potter, K. W., Wilcock, P. R. (Eds.), *Natural and Anthropomorphic Influences in Fluvial Geomorphology*. Geophysical Monograph, 89. American Geophysical Union, Washington, DC, 57–81, <https://doi.org/10.1029/GM089p0057>, 1995.
- 975 Naiman, R. J., Bechtold, J. S., Beechie, T. J., Latterell, J. J., & Van Pelt, R.: A process-based view of floodplain forest patterns in coastal river valleys of the Pacific Northwest, *Ecosystems*, 13, 1-31, <https://doi.org/10.1007/s10021-009-9298-5>, 2010.
- Nyberg, B., Henstra, G., Gawthorpe, R. L., Ravnås, R., & Ahokas, J.: Global scale analysis on the extent of river channel belts, *Nature Communications*, 14, 2163, <https://doi.org/10.1038/s41467-023-37852-8>, 2023.
- Pizzuto, J., Keeler, J., Skalak, K., & Karwan, D.: Storage filters upland suspended sediment signals delivered from watersheds,
980 *Geology*, 45(2), 151-154, <https://doi.org/10.1130/G38170.1>, 2017.
- Redner, S.: *A Guide to First Passage Time Processes*, 328 pp., Cambridge Univ. Press, New York. 2001.
- Repasch, M., Wittmann, H., Scheingross, J. S., Sachse, D., Szupiany, R., Orfeo, O., Fuchs, M., & Hovius, N.: Sediment transit time and floodplain storage dynamics in alluvial rivers revealed by meteoric ¹⁰Be, *Journal of Geophysical Research: Earth Surface*, 125, e2019JF005419, <https://doi.org/10.1029/2019JF005419>, 2020.
- 985 Repasch, M., Scheingross, J. S., Hovius, N., Lupker, M., Wittmann, H., Haghypour, N., Gröcke, D. R., Eglinton T. I., and Sachse, D.: Fluvial organic carbon cycling regulated by sediment transit time and mineral protection, *Nat. Geosci.*, 14, 842–848, <https://doi.org/10.1038/s41561-021-00845-7>, 2021.
- [Scheingross, J. S., Repasch, M. N., Hovius, N., Sachse, D., Lupker, M., Fuchs, M., Helevy, I., Gröcke, D. R., Golombek, N. Y., Haghypour, N., Eglinton, T. I., Orfeo, O., & Schleicher, A. M.: The fate of fluvially-deposited organic carbon during transient floodplain storage, *Earth and Planetary Science Letters*, 561, 116822, <https://doi.org/10.1016/j.epsl.2021.116822>, 2021.](https://doi.org/10.1038/s41561-021-00845-7)
- 990 <https://doi.org/10.1016/j.epsl.2021.116822>, 2021.

- Schumm, S. A., & Lichty, R. W.: Flood-plain construction along Cimarron River, in southwestern Kansas, Geol. Surv. Prof. Pap. 352-DUS Gov. Printing Office, Washington, 1963. 365
- 995 Skalak, K., & Pizzuto, J.: The distribution and residence time of suspended sediment stored within the channel margins of a gravel-bed bedrock river, *Earth Surface Processes and Landforms*, 35, 435-446, <https://doi.org/10.1002/esp.1926>, 2010.
- Tofelde, S., Bernhardt, A., Guerit, L., & Romans, B. W.: Times associated with source-to-sink propagation of environmental signals during landscape transience, *Front. Earth Sci.*, 9, 628315, <https://doi.org/10.3389/feart.2021.628315>, 2021.
- Tofelde, S., Bufe, A., & Turowski, J. M.: Hillslope sediment supply limits alluvial valley width, *AGU Advances*, 3, e2021AV000641. <https://doi.org/10.1029/2021AV000641>, 2022.
- 1000 Torres, M. A., Limaye, A. B., Lamb, M. P., West, A. J., & Fischer, W. W.: Model prediction of long-lived storage of organic carbon in river deposits, *Earth Surface Dynamics*, 5, 711-730, <https://doi.org/10.5194/esurf-5-711-2017>, 2017.
- Turowski, J. M., Bufe, A., & Tofelde, S.: A physics-based model for fluvial valley width, *Earth Surface Dynamics*, 12, 493-514, <https://doi.org/10.5194/esurf-12-493-2024>, 2024.
- Uhlenbeck, G. E., & Ornstein, L. S.: On the theory of the Brownian motion, *Phys. Rev.* 36, 823-841, <https://doi.org/10.1103/PhysRev.36.823>, 1930.
- 1005 van de Lageweg, W. I., van Dijk, W. M., & Kleinhans, M. G. (2013). Channel belt architecture formed by a meandering river. *Sedimentology*, 60(3), 840–859. <https://doi.org/10.1111/j.1365-3091.2012.01365.x>
- Wickert, A. D., Martin, J. M., Tal, M., Kim, W., Sheets, B., & Paola, C.: River channel lateral mobility: Metrics, time scales, and controls. *Journal of Geophysical Research: Earth Surface*, 118, 396–412. <https://doi.org/10.1029/2012JF002386>, 2013.

1010